Ore Geology Reviews 109 (2019) 50–78

Contents lists available at ScienceDirect

Ore Geology Reviews

journal homepage: www.elsevier.com/locate/oregeorev

Calcrete uranium deposits in the Southern High Plains, USA

S.M. Hall[a,*], B.S. Van Gosen[b], J.B. Paces[c], R.A. Zielinski[a], G.N. Breit[b]

[a] U.S. Geological Survey, Energy Resources Science Center, Box 25046, MS 939, Denver, CO 80225, USA
[b] U.S. Geological Survey, Geology, Geophysics and Geochemistry Science Center, Box 25046, MS 973, Denver, CO 80225, USA
[c] U.S. Geological Survey, Denver Radiogenic Isotope Lab, Box 25046, MS 963, Denver, CO 80225 USA

ARTICLE INFO

Keywords:
Uranium
Calcrete
Geochemistry
Finchite
Carnotite
Vanadium

ABSTRACT

The Southern High Plains (SHP) is a new and emerging U.S. uranium province. Here, uranyl vanadates form deposits in Pliocene to Pleistocene sandstone, dolomite, and limestone. Fifteen calcrete uranium occurrences are identified; two of these, the Buzzard Draw and Sulfur Springs Draw deposits, have combined in-place resources estimated at about 4 million pounds of U_3O_8. Ore minerals carnotite and finchite are hosted in dolomite at the Sulfur Springs Draw deposit, with accessory fluorite, celestine, smectite/illite, autunite, and strontium carbonate. Host carbonate at the Sulfur Springs Draw deposit is ~190 ka and mineralization mobilized as recently as 3.8 ka. Ash collected near the deposit is 631 ka and erupted from the Yellowstone caldera complex. The Triassic Dockum Group that contains sandstone-hosted uranium deposits throughout the region and underlies the SHP is a potential source for uranium and vanadium. Regional uplift and dissection reintroduced oxygenated groundwater into the Dockum Group, mobilizing uranium. Additional uranium may have been contributed to groundwater by weathering of volcanic ash in Pliocene and Pleistocene host rocks. The locations of the uranium occurrences are mostly in modern drainage systems in the southeast portion of the SHP. Modelling of modern groundwater in the SHP carried out in a parallel study shows that a single fluid could form carnotite through evaporation, and that fluids of the requisite composition are more prevalent in the southern portion of the SHP. The southeastern portion of the SHP hosts more uranium occurrences due to a variety of factors including (1) upward transport of groundwater and connectivity between source and host rock, (2) higher uranium and vanadium content of groundwater, (3) higher rates of groundwater recharge in this region to drive the mineralizing system, and (4) shallower groundwater facilitating surface evaporation. Ongoing erosion of host rocks challenges preservation of deposits and may limit their size.

1. World calcrete uranium deposits

Surficial uranium is a diverse category of deposits that are found in near-surface Tertiary to recent sedimentary rocks or soils worldwide (International Atomic Energy Agency, 2009). Five sub-types of surficial uranium deposits are recognized: (1) fluvial valley, (2) lacustrine-playa, (3) peat-bog, (4) karst cavern and (5) surficial pedogenic and structure fill deposits (Dahlkamp, 2010). The fluvial valley and lacustrine-playa sub-types are considered calcrete uranium deposits because of their association with near-surface carbonate rock (calcrete) and are the only deposit types considered in this study. Although some definitions of calcrete are restricted to carbonate that forms in response to pedogenic processes (Neuendorf et al., 2011), a broader usage of the term calcrete as either vadose or phreatic is accepted in Australia and southern Africa where most calcrete uranium deposits are found (Chen et al., 2002) and is used in this paper.

Calcrete uranium deposits have been identified on five continents (Fig. 1). These deposits are found in semiarid to arid regions, although climatic belts alone do not predict where deposits are located (Carlisle, 1983; Mann and Horwitz, 1979). In Namibia and Western Australia several calcrete uranium deposits are the focus of modern exploration and exploitation. Fifty-eight calcrete uranium deposits with reported grade and tonnage, and an additional 35 deposits without reported resources, have been identified in 15 countries (Hall and Mihalasky, 2017). The average grade of these deposits ranges from ~60 to ~1300 parts per million (ppm) U, averaging ~280 ppm U using cutoff grades between 17 and 425 ppm U. Total contained metal in world calcrete uranium deposits is from ~0.04 to ~190 million lb U_3O_8, averaging 14 million lb. U_3O_8. (Hall and Mihalasky, 2017). As compared with uranium deposits of most other types, calcrete uranium deposits are

* Corresponding author.
E-mail addresses: susanhall@usgs.gov (S.M. Hall), bvangose@usgs.gov (B.S. Van Gosen), jbpaces@usgs.gov (J.B. Paces), rzielinski@usgs.gov (R.A. Zielinski), gbreit@usgs.gov (G.N. Breit).

https://doi.org/10.1016/j.oregeorev.2019.03.036
Received 21 June 2018; Received in revised form 4 December 2018; Accepted 31 March 2019
Available online 03 April 2019
0169-1368/ Published by Elsevier B.V.

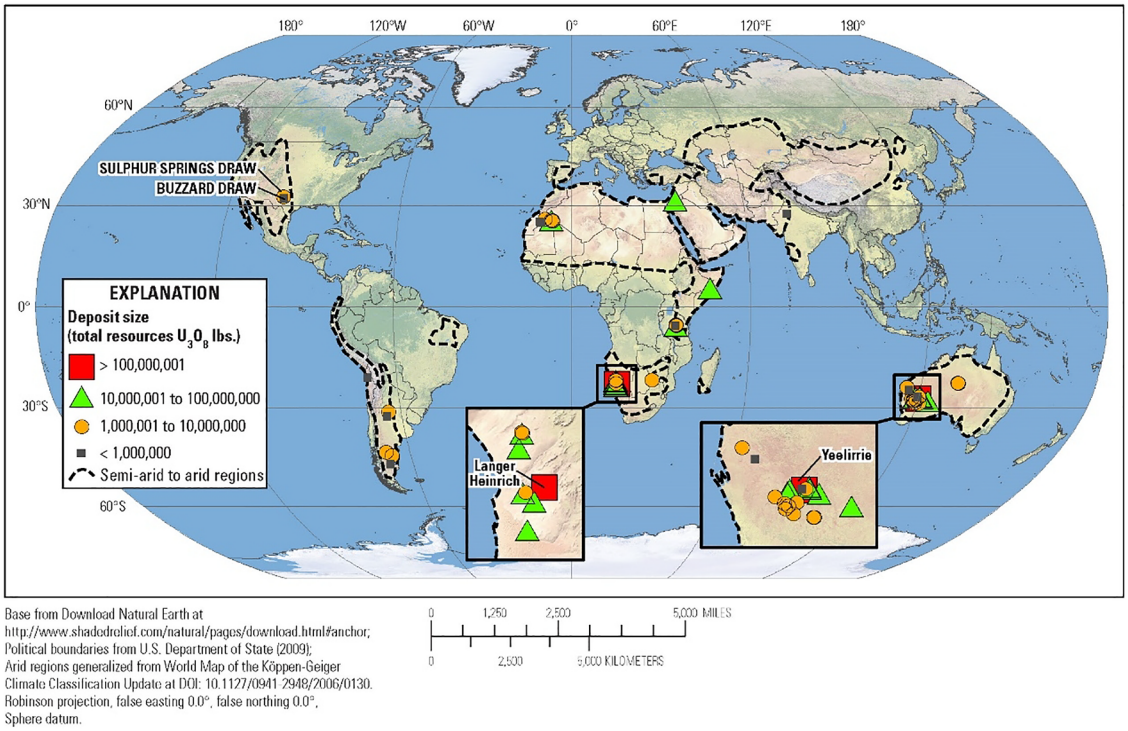


Fig. 1. Locations where calcrete uranium with economic resources have been reported.

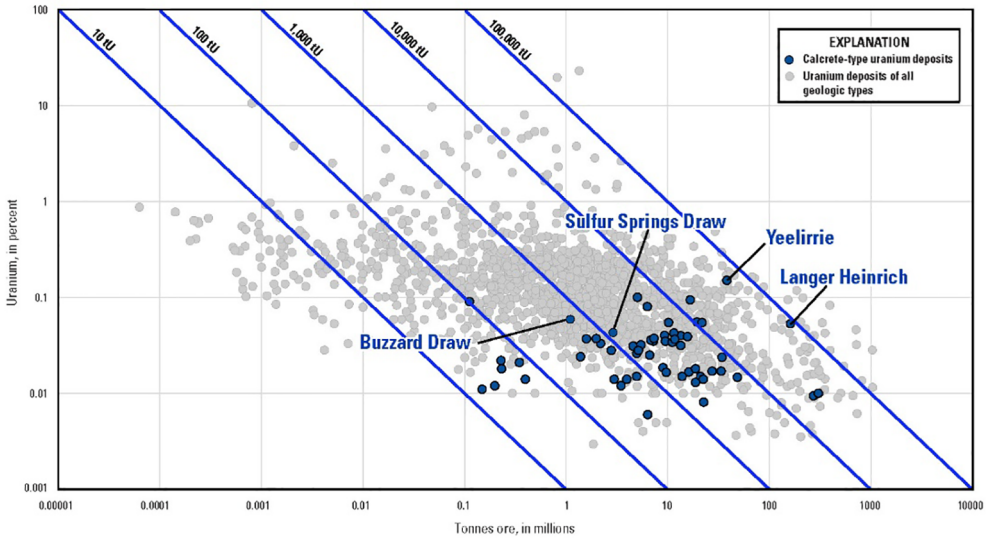


Fig. 2. Calcrete uranium deposits (blue) as compared with uranium deposits of all other types (Hall and Mihalasky, 2017; International Atomic Energy Agency, 2009). (For interpretation of the references to color in this figure legend, the reader is referred to the web version of this article.)

typically lower in average grade (Fig. 2). Although low grade, calcrete uranium deposits can be economic because they can be significant in size and are found near the surface, where they can be exploited with shallow open-pit mines.

1.1. Geologic setting

Deposits form within surface lacustrine and fluvial systems including lakes, channels, deltas and associated sedimentary facies. A single drainage can host multiple deposit types. In Australia, the Dawson and Hinkler Well fluvial-valley calcrete uranium deposits formed in the drainage that empties into Lake Way where playa type calcrete uranium deposits form in a chemical delta (Crabb et al., 1984). This illustrates the interconnected nature of calcrete uranium deposits in arid fluvial systems. Because they occur in a spectrum of facies within these sedimentary systems, it may be too simplistic to classify these deposits as either fluvial valley or lacustrine-playa, but this nomenclature persists.

Calcite and (or) dolomite are always associated with calcrete uranium deposits (Toens, 1984). Pedogenic carbonate (calcrete) horizons that form over broad regions as part of soil-forming processes in arid environments are not an indicator for uranium vanadate mineralization. In Western Australia, pedogenic calcrete is not found in the same region where calcrete uranium deposits are identified (Butt et al., 1977). However, in the Southern High Plains (SHP) pedogenic calcrete and non-pedogenic carbonate both occur, can grade into each other and are often difficult to distinguish in the field. Uranium mineralization is also found in siliciclastic sediments proximal to carbonate, with greater

concentration of ore minerals sometimes noted near the modern water table (Jaireth et al., 2015). At two of the largest deposits, Yeelirrie and Langer-Heinrich, sediments dominated by siliciclastics that lie below carbonate beds that cap the deposits contain most of the ore.

Worldwide, uranyl vanadates, principally carnotite with minor tyuyamunite, are the most common ore minerals. Uranyl silicates (soddyite, weeksite and uranophane), one uranyl phosphate mineral (metaautunite) and uranium within fluorescent opaline silica have also been reported, but these are not major constituents of ore (Butt et al., 1977; Butt and Graham, 1981; Pagel, 1984). Carnotite occurs as small disseminated grains, coatings on grains and carbonate nodules, matrix and vug fill, and coatings on slip and fracture planes. Gangue minerals include clays (palygorskite, sepiolite, smectite, illite, and kaolinite), fluorite, celestine, gypsum, halite, carbonates (calcite and dolomite with minor aragonite), and other siliciclastic minerals and lithic fragments that compose host rocks (Kinnaird and Nex, 2016; Pagel, 1984). Carnotite is strongly associated with palygorskite and montmorillonite at the Trekkopje deposit in Namibia (Kinnaird and Nex, 2016; Youlton, 2007). Although much of the mineral resource in calcrete uranium deposits can be hosted in siliciclastic rock, uranyl vanadates are the dominant ore mineral in calcrete uranium deposits but only a minor constituent of other more common types of sandstone-hosted uranium deposits. Both deposit types form from groundwater; calcrete uranium deposits form in response to evaporative conditions versus tabular or roll-front sandstone-hosted deposits that form through mechanisms of reduction and oxidation.

1.2. Climate, topography and hydrology

The climatic and hydrologic factors required to form calcrete uranium deposits include: (1) groundwater or surface water flow that is adequate to transport uranium; (2) local hydraulic conditions that create upward movement of groundwater; (3) slow moving flow; and (4) a prolonged arid climate favoring near-surface evaporation and preservation of deposits once they form (Carlisle, 1984). Surface- and groundwater flow in the portion of Western Australia in which calcrete deposits are found is intermittent through chains of saline lakes along fluvial channels that developed on subdued topography ranging between 150 and 500 m (Butt et al., 1977). In Namibia, deposits formed on the subdued topography of the Namib platform during the middle Tertiary to Pleistocene when the climate was less arid. The wetter transported significant uranium in groundwater and formed well-defined paleochannels (Carlisle, 1984; Kinnaird and Nex, 2016). Deposits form where variations in topographic gradient create upward movement of groundwater and (or) ponding of surface water allowing evaporation. At the Yeelirrie deposit, shallowing of the local topographic gradient from 0.12% to 0.06% correlates with mineralization (Cameron, 1984).

Most calcrete uranium deposits are in the Southern Hemisphere clustering around 32 degrees south latitude, with some outliers close to the equator in Tanzania (~5 degrees south) and Somalia (~5 degrees north), and another set of outliers at 43 to 47 degrees south in Argentina. Deposits in the Northern Hemisphere are rarer, and cluster around 25 degrees north (Hall and Mihalasky, 2017). The distribution of deposits probably relates to arid subtropical climatic belts that are common at these latitudes, with outliers formed within local arid regions caused by other factors such as rain shadow effects (Fig. 1). Both in Western Australia and Namibia, the deposits form in the interior of the continent beyond the influence of coastal moisture and away from storm tracks (Butt et al., 1977; Kinnaird and Nex, 2016).

1.3. Genetic models

Following a mineral systems approach, genetic deposit models for calcrete uranium deposits can be defined by determining uranium and vanadium sources, transport, trap, and the preservation potential for deposits. The source for uranium is most often attributed to felsic igneous rocks including granite, monzonite, and alaskite, which are inherently enriched in uranium (Jaireth et al., 2015). The sources of vanadium are typically attributed to weathered mafic minerals hosted in a variety of rock types that vary regionally, including mafic igneous rocks, iron formations, mafic-rich schists, greenstone belts, vanadium-rich clays, and ferruginous regolith (Hartleb, 1988; Mann and Deutscher, 1978). Both uranium and vanadium are liberated during uplift and exposure, accompanied by prolonged periods of physical and chemical weathering. Genetic models largely focus on sources of uranium and vanadium, as there is typically adequate potassium to form carnotite in exogenic environments.

Uranium and vanadium are transported to the site of deposition via groundwater flow which moves laterally and (or) vertically through ancient and modern channels and associated playas in near-surface sedimentary rocks (Carlisle, 1978). Genetic models are either single-fluid models, where uranium and vanadium are transported together, or models involving mixing of two fluids (Boyle, 1974; Mann and Deutscher, 1978). In a single-fluid model, uranyl vanadates precipitate in physical traps where groundwater evaporates in areas where hydrologic gradients decrease, such as in playas, or when flow is interrupted by changes in the direction of channels (Kinnaird and Nex, 2016; Mann and Deutscher, 1978; Youlton, 2007). In a fluid-mixing model, deposits form where uranium-rich water mixes with waters containing vanadium or potassium, or when mixing of waters results in decreasing pH, increased oxidation state, or lower partial pressure of CO_2, all of which favor the formation of uranyl vanadate ore minerals (Jaireth et al., 2015). Preservation of calcrete uranium deposits requires a sustained regional arid environment and a stable low-energy, low-gradient flow regime. Increased flow can dissolve or erode existing deposits.

2. Southern High Plains

In 2011, the U.S. Geological Survey (USGS) developed a framework to evaluate domestic uranium resources that were last assessed in the 1980s. This included ranking of regions or deposit types that had not been fully evaluated in the United States. Calcrete uranium was recognized as a high-priority deposit type that had not been thoroughly assessed. Calcrete uranium deposits were studied during the U.S. Department of Energy's National Uranium Resource Evaluation Program (NURE); however, no deposits were identified, and these studies did not result in a dedicated assessment (Carlisle, 1978; U.S. Department of Energy, 1980). USGS scientists recognized that the primary factors responsible for this type of deposit are found in arid regions of the southwestern United States and began a new study of the potential for calcrete uranium. Historical industry databases, not published before this investigation, confirmed that calcrete uranium deposits exist in the SHP region of the United States (Van Gosen and Hall, 2017). Based on those discoveries, an assessment of undiscovered calcrete uranium was completed using the genetic systems framework model presented here (Hall et al., 2017).

The SHP physiographic province is an approximately 80,000 km^2 elevated plateau bounded by erosional escarpments in northwestern Texas, southeastern New Mexico and western Oklahoma (Fig. 3). The surface of the SHP has low relief, ranging in elevation between about 1400 m in the northwest and about 900 m in the southeast. The water table mirrors the topography, and flow is directed to the southeast with an average hydraulic gradient of 1.9 m/km. The present-day climate is semiarid, with an average annual precipitation of between 330 and 560 mm, that increases from the west to east. Average annual evaporation is from 1800 to 2000 mm/year, increasing north to south along with average temperature (Scanlon et al., 2012; Wood, 2002). Over 20,000 small playa lakes, 40–50 large saline lakes, and several intermediate-sized playa lakes characterize the present-day SHP (Reeves, 1990; Wood, 2002).

Most of the region is capped by a 3- to 4-meter thick layer of

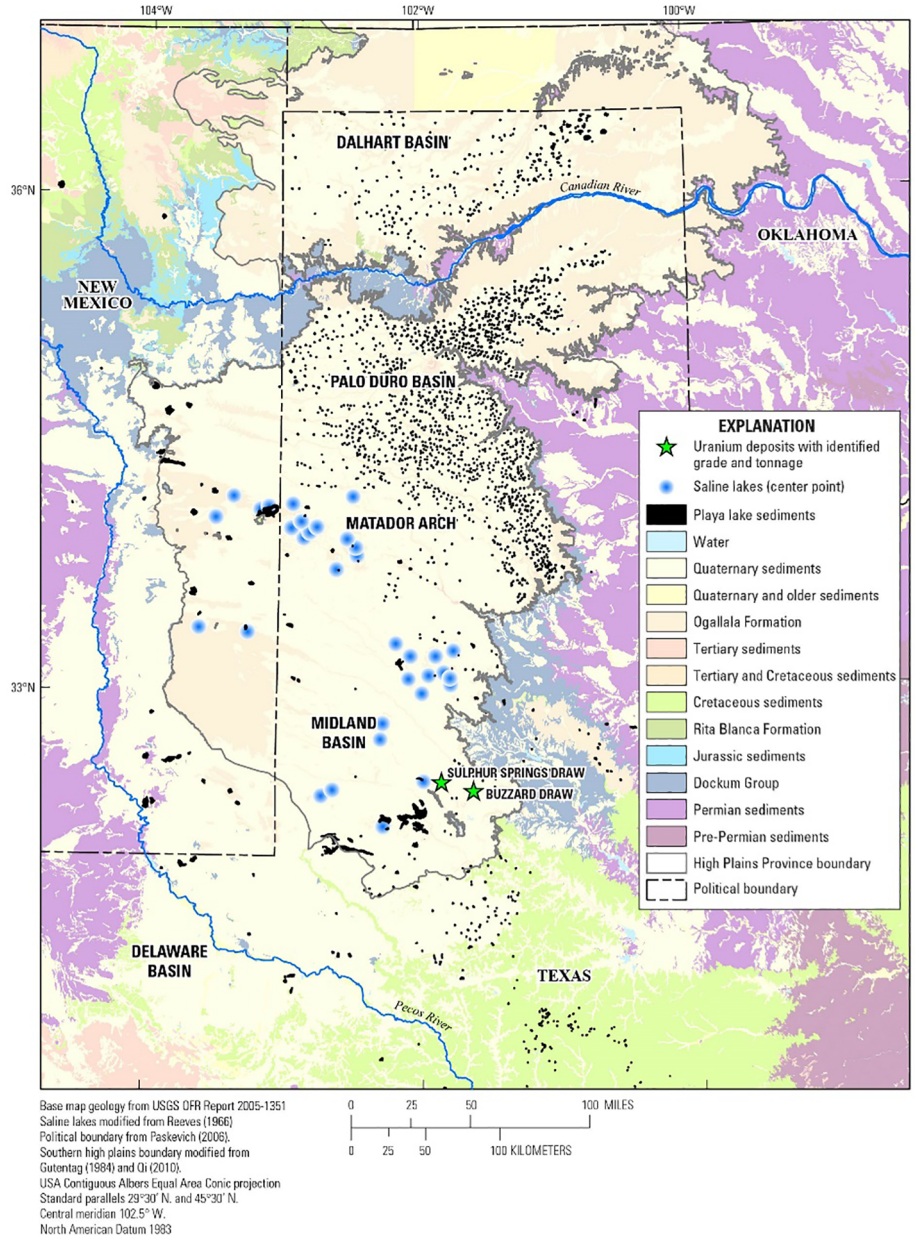


Fig. 3. Simplified geologic map of the Southern High Plains physiographic region, also showing saline and playa lakes. (See above-mentioned references for further information.)

pedogenic carbonate (caliche) that forms on the surface of underlying Pliocene and Pleistocene sediments (Reeves, 1970). Pedogenic carbonate in the SHP is mined in open pits for use as road building material. However, in genetic calcrete uranium deposit models, only non-pedogenic carbonate is associated with deposits. In the SHP, this includes rocks deposited in fluvial-lacustrine systems in the Miocene to Pliocene Ogallala Formation and Pleistocene sediments (Fig. 4).

2.1. Geology

Pliocene and Pleistocene sedimentary rocks present at the surface of the SHP were deposited on a surface of eroded Cretaceous and Triassic sandstones and carbonate rocks that crop out on the margins of the SHP plateau (Figs. 3–6) (Eifler et al., 1974).

2.1.1. Upper Triassic Dockum Group

The Dockum Group accumulated in several individual Paleozoic intracratonic structural basins that underlie the SHP. Beds dip gently towards the center of the Midland Basin where they display a maximum thickness of about 600 m (McGowen et al., 1977). The Dockum is overlain by Jurassic rocks in the northwest portion of the SHP and by Cretaceous rocks in much of the rest of the SHP. However, both Jurassic and Cretaceous units are missing in portions of the SHP. In those areas, the Miocene to Pliocene Ogallala Formation directly overlies the Dockum (Figs. 5 and 6). The Dockum is mostly siliciclastic sediments; the lower and middle portions are more porous and permeable and constitute regional aquifers (Bradley and Kalaswad, 2003). Recharge is from overlying units in the northern portion of the SHP and underlying units in the southern portion of the SHP.

2.1.2. Cretaceous strata

Cretaceous rocks include thin to massive sandstones, shale, sandstone, and marl up to 75 m thick in the northern portion of the SHP, and 30 m thick in the southern portion (Nativ and Gutierrez, 1989). There are two major Cretaceous aquifers: the (1) the Antlers Sand, typically under artesian pressure; and (2) the Comanche Peak and Edwards

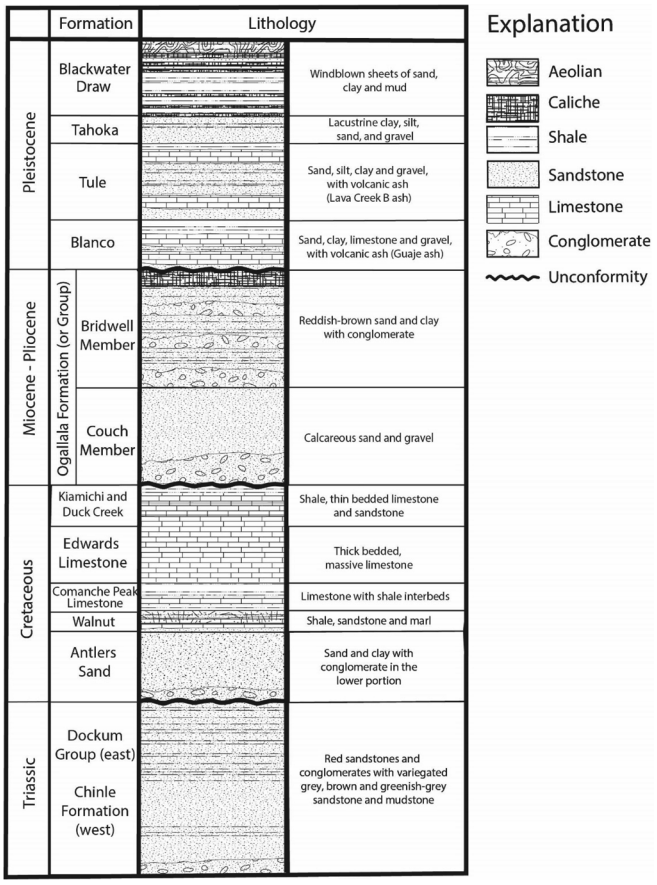


Fig. 4. Stratigraphic column showing geologic units of Triassic age and younger exposed in the Southern High Plains (Bradley and Kalaswad, 2003; Eifler, 1967; Eifler et al., 1974; Holliday, 1989; Lucas and Anderson, 1995; Nativ and Gutierrez, 1989).

Limestones (Fallin, 1989). Recharge to the Lower Cretaceous aquifers is from the overlying Ogallala Formation. Discharge is to streams, springs and seeps throughout the SHP and into adjacent sedimentary units (Fallin, 1989)

2.1.3. Miocene-Pliocene Ogallala Formation

The Ogallala Formation (or Group) was deposited in a series of alluvial fans and channels that trended southeast and cut into underlying Cretaceous strata (Nativ and Smith, 1987). The thickest portion of the Ogallala in the SHP is about 250 m thick in the axes of major drainage systems developed in the northern portion of the region. In the late Pliocene, the Pecos and Canadian River drainage system changed (Fig. 3), cutting off sediment flow to the SHP, and thus ending deposition of the Ogallala (Wood, 2002).

The Ogallala aquifer is the main water source for the SHP and extends beyond the region to form the largest aquifer system in the United States. Recharge varies throughout the region. In places, recharge is upward from the Dockum Group and Cretaceous strata, and in places downward from younger units (Reedy et al., 2003). Natural discharge is through evaporation, transpiration, and through seeps and springs, mostly on the eastern escarpment of the SHP. Before agricultural development (crop irrigation) in the 1930s, groundwater discharged along the eastern escarpment and into many of the major drainages in the region (Wood, 2002). Pumping of groundwater for agricultural use, and perhaps contributions from climate changes during the Holocene, have lowered the level of groundwater in most of the SHP (Scanlon et al., 2012). Groundwater levels fell a mean of 11 m in Texas, and more than 50 m in the northern portion of the SHP between 1950 and 2007 (Scanlon et al., 2012). Many historical springs that were found throughout the SHP in the early 1900s no longer flow (Nativ and Smith, 1987). However, due to changes in land use, the southeast portion of the SHP records increased water levels of 3–20 m (Scanlon et al., 2012).

2.2. Pliocene and Pleistocene volcanic ash

Volcanic ash has been identified in the Ogallala Group and Tule Formation (Guaje Pumice Bed, 1.4 Ma; Blanco Formation; Lava Creek B ash, 0.64 Ma, Tule Formation) accumulated on the Ogallala surface (Fig. 4) (Frye and Leonard, 1957; Holliday, 1989; Izett, 1981). Volcanic ash collected from the Sulfur Springs Draw deposit was analyzed by the USGS Tephrochronology Project. The sample was analyzed using electron microprobe microanalysis to determine nine major and minor oxides. The ash consists of moderately to well-hydrated (~93% total) glass with a composition that is well correlated with distal Lava Creek B ash previously identified throughout the western United States (Table 1). The Lava Creek B ash erupted at 631 ± 4 ka (Matthews et al., 2015), and based on the age and composition, the eruptive source is the Yellowstone caldera Complex.

2.2.1. Pleistocene to Holocene strata

Numerous small channels developed on the surface of the Ogallala Formation during the Pleistocene and filled with sediments deposited in alternating wet and dry cycles. Pleistocene and Holocene strata are discontinuous and highly variable in thickness. They range to as much as an average cumulative thickness of about 100 m. No major aquifers are defined in Pleistocene to Holocene strata in the SHP.

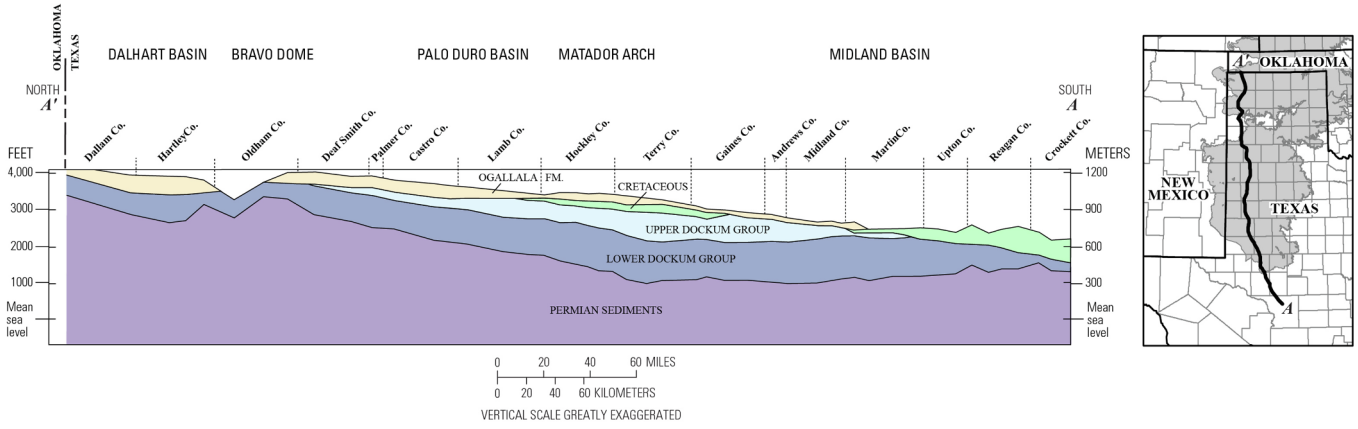


Fig. 5. North-South cross section through the central portion of the Southern High Plains region. Modified from McGowen et al. (1977).

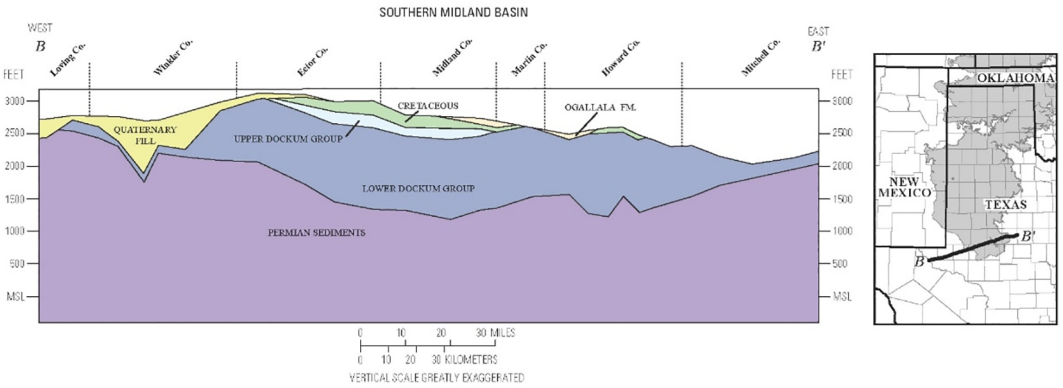


Fig. 6. West-East cross section through the southern portion of the Southern High Plains region. Modified from McGowen et al. (1977).

2.2.2. Quaternary calcrete

Periodic arid climate conditions and low sediment influx into the SHP resulted in thick pedogenic calcrete soil horizons forming on Ogallala and Pleistocene to Holocene sediments. The thickness and extent of pedogenic calcrete is an important control on local and regional rates of groundwater recharge in the SHP. Pedogenic calcrete is not found beneath many playas and where identified is thin and sandy, both scenarios favor downward transport of water to recharge regional aquifers (Gurdak and Roe, 2010). Interplaya recharge where pedogenic calcrete is thicker is less important, but still significant. Calcrete is thickest (up to 1.3 m) in the northern portion of the SHP where groundwater recharge is lowest, and thinnest in the southwestern portion of the SHP where recharge is highest (Knowles et al., 1984).

3. Calcrete uranium occurrences in the Southern High Plains

Fifteen calcrete uranium occurrences were identified in the SHP through regional evaluation by the U.S. National Uranium Resource Evaluation Program (NURE), USGS, and exploration by the Kerr-McGee Corporation (Finch, 1975; Krish, 1977b; McGowen et al., 1981) (Fig. 7, Table 2). These occurrences include unmined (currently subeconomic) deposits, prospects, showings, and geochemical or geophysical anomalies, some of which were drill tested by the Kerr-McGee Corporation. Precise locations of the occurrences were not always available in Kerr-McGee company reports and maps. Therefore, locations given in Table 2 and Fig. 7 should be considered approximate.

3.1. Historical evaluation

3.1.1. U.S. government evaluation for calcrete uranium

The potential for uranium deposits in the SHP was evaluated by USGS geologists in the 1970s, and the U.S. Department of Energy as part of the NURE program (U.S. Department of Energy, 1980). Favorable areas for calcrete uranium were identified in the Tule and Ogallala Formations in the Lubbock quadrangle, and one occurrence, Lott (Fig. 7) was sampled (Table 2) (McGowen et al., 1981). The Tule Formation is considered favorable for potential deposits because of identified occurrences, high average values of uranium in rock samples, and volcanic ash (which represents a potential source rock for uranium) in this unit. Pedogenic carbonate developed on the Ogallala Formation contains about 2.5 ppm U (Finch, 1975), but opalized conglomerate in the Ogallala containing up to 50–100 ppm U is described in the Plainview quadrangle (Amaral, 1979). Radiometric anomalies were recognized in the NURE airborne radiometric surveys near some playa lakes, and exposed portions of the Slaton and Sulfur Springs Draw occurrences. Radiometric anomalies in playa lakes were not considered an indicator of favorable areas because of the limited extent and thickness of sediment in these lakes.

3.1.2. Kerr-McGee Corporation exploration program

From 1973 to 1981, the Kerr-McGee Corporation explored for calcrete uranium in the SHP, choosing this region based on similarities to Western Australia where calcrete uranium had been recently discovered. Internal company correspondence, maps, and reports that were recently released to the USGS formed the basis for the following summary of their exploration program. Kerr-McGee used a combination of geophysical and geochemical surveys to identify prospective areas. The region was explored using the proprietary ARDA (Airborne Radiometric Detection Apparatus) technique. Anomalies were then verified using commercial Mount Sopris airborne radiometric instruments flying at lower altitude, and finally by ground radiometric surveys. Anomalous gamma signatures in oil well logs drilled through Pliocene or Pleistocene rocks were also compiled. The company used alpha-track methods to survey for anomalous radon in surface soils to identify prospective areas but did not find this method effective. Groundwater samples were collected and analyzed for dissolved uranium. The samples were also analyzed for dissolved sulfate and salinity to evaluate the contribution of evaporative concentration. The company completed orientation surveys of helium over known mineralized portions of the SHP as a measure of local radioactive decay.

Table 1
Microprobe analysis of Lava Creek B ash collected near the Sulfur Springs Draw Deposit normalized to 100%

	Na_2O	MgO	Al_2O_3	SiO_2	K_2O	CaO	TiO_2	MnO	FeO	Total
Mean	2.841	0.015	12.443	77.367	5.282	0.518	0.0833	0.0400	1.4098	100
Std Deviation	0.202	0.011	0.126	0.251	0.381	0.042	0.0462	0.0259	0.1716	0
Minimum	2.440	0.000	12.109	76.894	4.850	0.408	0.0000	0.0000	1.1830	100
Maximum	3.173	0.033	12.647	77.807	6.210	0.605	0.1756	0.0867	1.7516	100
Range	0.732	0.033	0.539	0.913	1.360	0.197	0.1756	0.0867	0.5685	0
Count	29	29	29	29	29	29	29	29	29	29
Confidence (95.0%)	0.073507	0.004065	0.045845	0.091428	0.138609	0.015217	0.016819	0.009428	0.062466	

Sample collected at latitude 32.45244°N, longitude −101.86386° (± 15 ft. accuracy), 2670 ft. elevation, Pleistocene Tule Formation, Martin County, Texas.

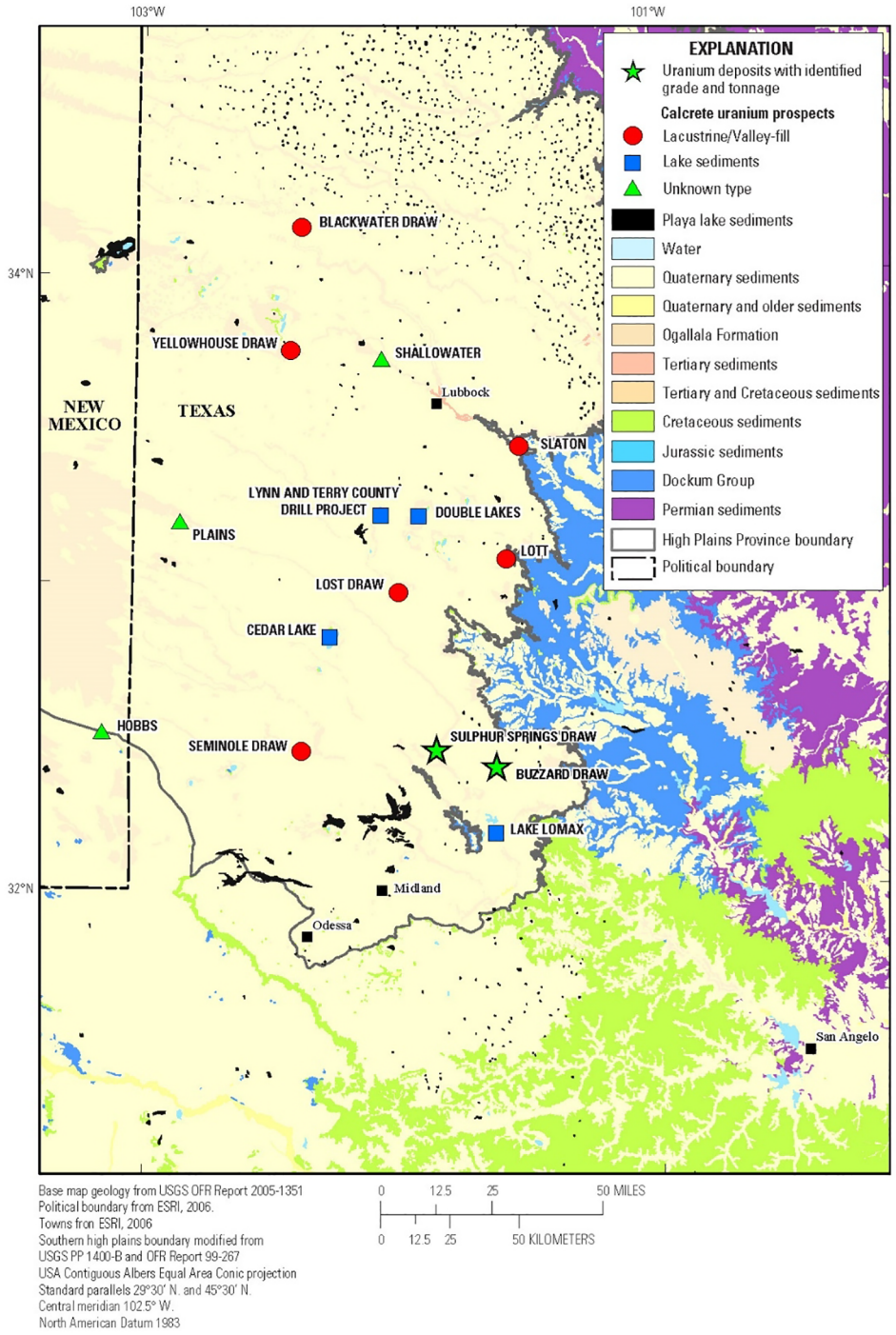


Fig. 7. Calcrete uranium occurrences in the Southern High Plains based on the work of Finch (1975), Krish (1977b) and McGowen et al., (1981).

Helium results were compromised by an overprint of petroleum-related helium anomalies and this effort was abandoned. Ultimately, Kerr-McGee identified 14 prospective areas within the SHP, and some were tested by drilling hundreds of shallow (< 30 m) holes (Fig. 7, Table 2).

3.1.3. Kerr-McGee deposit model

The company identified three types of uranium occurrences in the SHP: (1) small, low-grade occurrences in silicified pedogenic calcrete developed on the Miocene to Pliocene Ogallala Formation; (2) small, low-grade occurrences hosted in middle- to late-Pleistocene lake sediments; and (3) potentially economic concentrations of uranium in Pleistocene non-pedogenic calcrete developed in valley-fill and lacustrine sediments (Holmberg and Kirsh, 1977). Their exploration focused on higher-grade deposits formed in early Pleistocene host rocks (i.e., type 3) as having the highest potential. Of interest were Pliocene sediment-filled paleovalleys that provided long-term channeling of potential mineralizing solutions (groundwater and surface water) and potential sites of evaporation (Schurman, 1981).

As the exploration program matured and geologists developed better understandings of the distribution of mineralization, the company targeted mixing zones between saline and fresh groundwater. They determined that a positive indicator for calcrete uranium deposits was the presence of sulfates, principally gypsum, in potential host rock, as well as high-sulfate groundwater that would indicate significant amounts of evaporation. Exploration targets focused on regions where calcium carbonate was deposited in drainages, evaporative lakes, and

Table 2
Uranium occurrences in the Southern High Plains, Texas.

Occurrence*	Source	Characteristics	Targeting Criteria	Evaluation
Lacustrine and Valley Fill Occurrences				
Blackwater Draw	Kerr-McGee Internal Correspondence	Lacustrine and valley-fill complex.	High sulfate in groundwater (no value provided), and uranium up to 340 ppb.	None reported
Buzzard Draw	Kerr-McGee Internal Correspondence	Mineralization in siltstone and sandstone near the contact with the underlying Dockum Group. Historic resources in all categories are 2.1 million tons @ 0.059% U_3O_8 containing 1.4 million pounds U_3O_8 (Krish, 1977a).	Identified by a detailed groundwater survey containing up to 700 ppb uranium. Surface exposures in Buzzard Creek contain up to 0.013% U_3O_8.	Mineralization delineated by at least 305 (< 100 ft.) drill holes.
Lost Draw	Kerr-McGee Internal Correspondence	Found in a northwest trending lacustrine and valley-fill sequence that may have included pluvial lakes.	Uranium in groundwater up to 210 ppb, sulfate to 3500 ppm.	None reported
Seminole Draw	Kerr-McGee Internal Correspondence	Lacustrine and valley-fill sediments contain up to 0.04% U_3O_8 in surface outcrops. Visible carnotite is reported as fracture and vug fillings and coatings on sand grains in both lacustrine and valley-fill sediments. The lacustrine and valley fill complex extends northwest to southeast about 28 miles and is about 12 miles wide.	Uranium in groundwater up to 100 ppb and sulfate to 2800 ppm.	None reported
Slaton Area	Kerr-McGee Internal Correspondence	Mineralization was identified in conglomeratic channel fill within the Ogallala Formation. The mineralized rock was within a small side channel feeding a large paleochannel filled with conglomerate, some boulder-sized, within the Ogallala Formation. Drilling confirmed that this deposit was an erosional remnant, much of the deposit eroded by the Double Mountain Fork of th eBrazos River.	A strong ARDA anomaly at the edge of the Ogallala caprock was confirmed by a ground radiometric survey. Visible carnotite was identified in outcrop.	27 shallow (< 100 ft.) holes drilled in fences. The best mineralization was near the outcrop.
Sulfur Springs Draw	Kerr-McGee Internal Correspondence	Mineralization in calcareous mudstones, siltstones and sandstones. Historic resources in all categories are 3.1 million tons @ 0.043% U_3O_8 containing 2.7 million pounds U_3O_8 (Krish, 1977a).	Strong ARDA anomaly and visible carnotite where rock crops out along Sulfur Springs Draw. Surface samples contained up to 0.05% U_3O_8. Grounwater near the deposit contained up to 240 ppb uranium, and 2900 ppm sulfate.	Mineralization delineated by over 669 (< 100 ft.) drill holes.
Yellow House Draw	Kerr-McGee Internal Correspondence	Lacustrine and valley-fill sediments are anomalous in uranium along the Yellow House Draw drainage.	Uranium in groundwater up to 240 ppb, sulfate to 2900 ppm, and gamma anomalies noted in local oil well logs.	None reported
Lott	McGowen and others, 1981	Outcropping Tule Formation and underlying Ogallala Formation that contains anomalous uranium.	Up to 0.013% U_3O_8 in Tule Formation, and 0.002% U_3O_8 in the underlying Ogallala Formation.	None reported
Lake Sediments				
Cedar Lake	Kerr-McGee Internal Correspondence	Mineralization of 0.003 to 0.004% U_3O_8 in dolomitic lake sediments (clays and silts) with associated gypsum.	String of 9 ARDA anomalies confirmed by lower altitude surveys completed using Mt. Sopris instruments and ground radiometric surveys.	Drill tested in 1974, no results reported.
Double Lakes	Kerr-McGee Internal Correspondence	Carnotite identified within lake sediments at Double Lakes and along a tributary in the eastern portion of the area.	High Chloride and Nitrate content in groundwater.	None reported
Lake Lomax	Kerr-McGee Internal Correspondence	Gypsum-rich clay and silt lake sediments are weakly mineralized, containing 0.01 to 0.05% U_3O_8.	Numerous point source ARDA and Mt. Sopris geophysical anomalies over present day lake beds. No point anomalies were identified in ground radiometric surveys.	Drill tested, no results reported
Lynn and Terry Counties	Kerr-McGee Internal Correspondence	Geochemical and geophysical anomalies in lake sediments in this region.	Groundwater samples contain up to 350 ppb uranium.	122 holes drilled in a grid pattern over 7 areas in Lynn and Terry Counties in 1979. All but 9 holes were barren.
Unknown Deposit Type				
Hobbs	Kerr-McGee Internal Correspondence	Unknown host rock.	Clustering of ARDA anomalies and surface mineralization reported in a caliche pit near Hobbs.	None reported
Plains	Kerr-McGee Internal Correspondence	Unknown host rock exposed in Sulfur Springs Draw.	Three ARDA anomalies along Sulfur Springs Draw	Ground radiometric surveys confirmed airborne geophysical anomalies.
Shallowater	Kerr-McGee Internal Correspondence	Unknown host rock.	Groundwater anomalies, up to 250 ppb uranium, and surface radiometric anomalies.	None reported

* Occurrences include unmined deposits, prospects, showings and geochemical or geophysical anomalies that may indicate the presence, tested or not, of economic quantities of uranium.

zones of evapotranspiration where the water table is close to the land surface. Lateral flow of groundwater capable of transporting large quantities of mineralizing solutions was thought to be a more important factor in forming economic deposits than vertical groundwater flow. Vertical groundwater flow results in pedogenic calcrete with sub-economic concentrations of uranium. The highest grades of mineralization at the Sulfur Springs Draw, Seminole Draw, Yellow House Draw, and Lost Draw occurrences were present at the boundary between lacustrine and valley-fill facies, where uranyl vanadates, carbonate minerals, and gypsum formed as groundwater evaporated and (or) mixed with groundwater of a different composition (Krish, 1977b).

3.2. Calcrete uranium deposits

Kerr-McGee identified two deposits in the SHP: The Sulfur Springs Draw and Buzzard Draw deposits (Fig. 7, Table 2). Together, the deposits contain historical in-place resources of about 3.9 million lb. U_3O_8 in demonstrated (measured, indicated, inferred) and "potential" resource categories (2.6 million lb recoverable U_3O_8 based on drawing pit limits around contiguous ore occurrences) (Hall and Mihalasky, 2017; Holmberg and Kirsh, 1977; Van Gosen and Hall, 2017; Wetz and Reyher, 1981).

The two deposits contain uranium hosted in calcareous mudstones, siltstones, and fine-grained sandstones that are currently above the modern water table. Host sediments are up to 30 m thick and are capped by unmineralized pedogenic calcrete up to 6 m thick (Van Gosen and Hall, 2017). Volcanic ash collected from rocks that host the Sulfur Springs Draw deposit is identified as Lava Creek B ash, therefore the age of host rock is 631 ka or younger.

Ore horizons at both deposits were determined using a cutoff grade of ~250 ppm U. The deposits in the SHP have the highest cutoff grade reported for global calcrete uranium deposits after Yeelirrie (425 ppm U); average cutoff grade for all global calcrete uranium deposits is 135 ppm U (Hall and Mihalasky, 2017). Mineralized rock averages 3.4 m thick and is present between 0 and 20 m below the surface (Waechter, 1974). At Sulfur Springs Draw, the ore occurs as irregular pods scattered over about 3 km^2, with anomalously high uranium concentrations in rock samples forming a larger halo covering 16 km^2 (Waechter, 1974). Ore-grade mineralization (360 ppm U) is on average 1.5 m thick, conforms to bedding, and is concentrated in calcareous mudstone (Waechter, 1974). The Sulfur Springs Draw deposit contains an estimated 2.7 million lb of U_3O_8 (2.8 million tonnes with an average grade of 0.036% U) in place in all historical resource categories. The Buzzard Draw deposit comprises pods of mineralization over about 2.4 km^2, defined by conformable sheets of ore-grade (500 ppm U) mineralization averaging about 1 m thick. Buzzard Draw contains an estimated 1.4 million lb of U_3O_8 (1.0 million tonnes with an average grade of 500 ppm U) in place in all historical resource categories (Krish, 1977a).

Calcrete uranium occurrences in the SHP are hosted primarily in the Ogallala Formation (Seminole Draw and Slaton prospects), and to a lesser extent in the Tule Formation (Sulfur Springs Draw deposit) and other Pleistocene rocks (Table 2) (Van Gosen and Hall, 2017). Surface sampling and subsurface drilling of calcrete uranium occurrences throughout the region identified mineralized rock that contains from 200 to 9500 ppm U (Barczak, 1974, Fallis, 1973).

3.2.1. Mineralogy and paragenesis

Uranyl vanadates visible in outcrop are rare in the SHP, and in places obscured by surface cultivation. Mineralized samples were collected by the USGS (Van Gosen and Hall, 2017) from one locale, the Sulfur Springs Draw Deposit, in Martin County, Texas where uranyl vanadates are exposed along a farm trench (Fig. 8, Table 2). Here, bright yellow uranium vanadate minerals form disseminations, root trace fillings, coat pebbles, fill fractures, and coat slickenside surfaces in calcareous siltstones and sandstones. Composite grab samples contain between 100 and 245 ppm U, and from 73 to 107 ppm V (Van Gosen and Hall, 2017).

Semi-quantitative energy-dispersive X-ray spectroscopy (EDAX) of mineral phases (Appendix A) identified dolomite, celestine, fluorite,



Fig. 8. Photographs of radioactive yellow mineralization collected from surface outcrops at the Sulfur Springs Draw deposit (hand lens and head of rock hammer are both approximately 25 mm). Photographs by Susan Hall.

Table 3
Paragenesis of minerals identified at the Sulfur Springs Draw Deposit, Texas.

Mineral Species	Formula*	Time
Microcrystalline Dolomite	$CaMg(CO_3)_2$	
Celestine	$SrSO_4$	
Carnotite	$K_2(UO_2)_2(VO_4)_2 \cdot 3H_2O$	
Smectite or Illite	$K_{0.65}Al_{2.0}[Al_{0.65}Si_{3.35}O_{10}](OH)_2$	
Finchite	$Sr(UO_2)_2(V_2O_8) \cdot 5H_2O$	
Fluorite	CaF_2	
Sr-Carbonate	$[SrCa?]CO_3$	

*Mineral formulas from www.mindat.org accessed June 15, 2016, with the exception of Finchite designated a new mineral by the International Mineralogical Association commission on new minerals, nomenclature and classification 10 August, 2017 (IMA No. 2017-052:http://nrmima.nrm.se/CNMNC39%28MM%29.pdf)

*Mineral formulas from www.mindat.org accessed June 15, 2016, with the exception of Finchite designated a new mineral by the International Mineralogical Association commission on new minerals, nomenclature and classification 10 August 2017 (IMA No. 2017-052:http://nrmima.nrm.se/CNMNC39%28MM%29.pdf).

smectite or illite, carnotite, a new uranium-vanadate mineral (finchite), and a strontium carbonate. The apparent mineral paragenesis based on petrological/mineralogical examination of the samples is summarized in Table 3. Autunite was identified by whole rock X-ray diffraction analysis (XRD) but was not observed during finer-scale EDAX analysis and could not therefore be placed into the paragenetic sequence. Finchite is an orthorhombic strontium-bearing uranyl vanadate with the ideal formula $Sr(UO_2)_2(V_2O_8)\cdot 5H_2O$, identical in structure to francevillite, curienite and metatyuyamunite. Finchite contains minor K, Ca, Mg, Al, and Fe substituting for Sr. The composition of carnotite and finchite were confirmed using an electron microprobe. Finchite was further characterized using spectroscopy, and by directly measuring crystallography and optical properties using single-crystal XRD (Spano et al., 2017). The composition of the strontium carbonate as measured by EDAX is close to strontianite in composition with a Ca:Sr ratio of 1.3 rather than 1, with some Ca attributable to dolomite inclusions. Apart from more detailed analysis of carnotite and finchite, the mineralogy described below was based on coupled scanning electron microscope and EDAX analysis.

Dolomite is micritic, most grains are less than 5 μm in diameter. In some cases, dolomite grains are zoned with strontium-rich cores and rims that contains trace aluminosilicates (Fig. 9A). Subrounded clastic grains and lithic fragments averaging about 25 μm in diameter are present, but not abundant. Early stage carnotite (< 1 to as much as 10 μm in diameter) fills pores within dolomite (Fig. 9B), with more abundant disseminations in more porous regions (Fig. 9C). Early stage carnotite does not contain detectable strontium, in contrast to later stage uranium vanadate mineralization that is Sr-rich. Celestine replaces and includes micritic dolomite and is a precursor to some carnotite growth (Fig. 9D), but also includes finchite indicating celestine continued to form throughout uranium mineralization (Fig. 9E). Layer silicates (either smectite or illite) fill porosity in dolomite (Fig. 9F). It is unclear if smectite/illite formed before or after carnotite. Later stages of carnotite are present as abundant disseminations and masses accompanied by bladed and tabular finchite (Fig. 9C, E, G, H, I). A late stage strontium carbonate forms crusts on the surfaces of dolomite (Fig. 9H). Paragenetically late fluorite lines vugs within dolomite (Fig. 9J).

Descriptions of the mineralogy of other calcrete uranium occurrences elsewhere in the SHP are similar to the Sulfur Springs Draw deposit. Carnotite, tyuyamunite, gypsum, illite, and kaolinite are reported to be hosted in dolomite and calcite (Barczak, 1974). Uranium and carbonate minerals are very fine grained (< 5μm), and dolomitic host rocks contain more uranium than limestone. Uranium-vanadate minerals in samples collected at the surface are finer grained than those in samples collected from the subsurface (Barczak, 1977).

The mineralogy of the Sulfur Springs Draw deposit is also similar to that of other global calcrete uranium deposits. Carnotite is ubiquitous at all deposits. Celestine is also identified at the Yeelirrie deposit in Australia and the Langer Heinrich and Tumas River deposits in Namibia (Pagel, 1984). Uranium is adsorbed into strontianite at the Bahi Swamp deposit in Tanzania (Bianconi and Borshoff, 1984); fluorite is described at the Lake Austin (Australia) and Tumas River (Namibia) deposits (Pagel, 1984). Smectite and dolomite are identified at Lake Way and Lake Maitland (Australia) (Pagel, 1984).

In contrast, the pervasiveness of strontium minerals observed at the Sulfur Springs Draw deposit is not reported for other calcrete uranium deposits. Modern saline lake water in the SHP contains 1.5 to 105 ppm Sr (Scanlon et al., 2009), and groundwater up to 85 ppm Sr in the SHP (National Water Information System, 2017) compared to typical groundwater in the United States that contains < 1 ppm Sr (Skougstad and Horr, 1963). Considering the regionally elevated concentrations of Sr dissolved in SHP water, it is reasonable that strontium-rich minerals are identified at the Sulfur Springs Draw deposit.

3.2.2. *Strontium isotope geochemistry*

Radiogenic strontium isotope ratios ($^{87}Sr/^{86}Sr$) were determined on samples of lacustrine dolomite host rock and associated carnotite-rich fracture coatings, as well as unmineralized carbonate-rich rocks from outside the main Sulfur Springs Draw mineralized zone (Table 4; Fig. 10a). Descriptions of samples analyzed (including photographs), analytical methods, and an assessment of data quality are presented in Appendix A. Values of $^{87}Sr/^{86}Sr$ for subsamples of several fragments of micritic host dolomite (SSD15-01) span a narrow range from 0.70849 to 0.70851 (n = 4). Results for individual aliquots fall within analytical uncertainty of the median value of 0.708500 ± 0.000016 (2σ). Carnotite-rich mineralization scraped from fracture surfaces cutting the same host material has a statistically identical median value of 0.708498 ± 0.000027 (2σ, n = 3) implying a single source of Sr in this sample (SSD15-01). Samples of materials collected from outside the mineralized zone (SSD15-02 to 06 in Table 4) have a larger range of $^{87}Sr/^{86}Sr$ values (0.708516 to 0.708604) and a slightly higher median value of 0.708543 ± 0.000064 (2σ). The median $^{87}Sr/^{86}Sr$ for all 16 analyses from Sulfur Springs Draw deposits is 0.70852 ± 0.00007. Very little mass-dependent fractionation occurs between Sr isotopes in response to near- surface chemical and physical processes. Therefore, the $^{87}Sr/^{86}Sr$ composition of the carbonate-rich Sulfur Springs Draw samples reflects the value present in the water at the time those minerals formed.

For comparison, $^{87}Sr/^{86}Sr$ analyses for groundwater and surface water collected from various localities throughout the SHP were compiled from the U.S. Geological Survey National Water Information System database (Table 5) (National Water Information System, 2017). Water samples were grouped by aquifer or rock formation from which they were obtained, and the distribution of $^{87}Sr/^{86}Sr$ values was used to evaluate possible sources contributing to mineralizing solutions at Sulfur Springs Draw (Fig. 10b). Median $^{87}Sr/^{86}Sr$ values ranged from

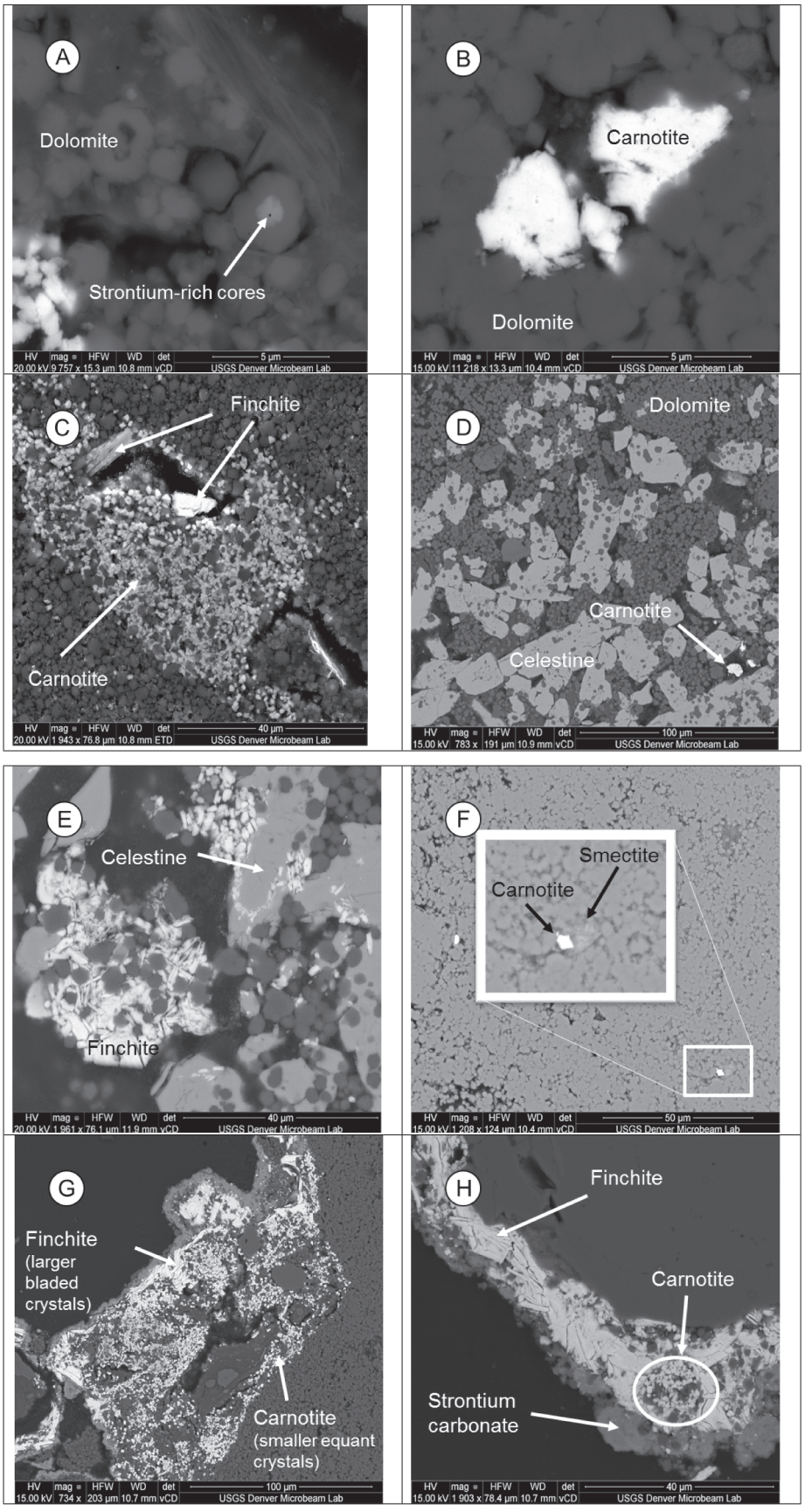


Fig. 9. SEM backscatter images of samples from the Sulfur Springs Draw deposit, scale shown on each image. A) Dolomicrite with examples of lighter colored, strontium-rich cores; B) Early stage carnotite in pores of dolomicrite; C) Disseminated carnotite and bladed finchite filling vugs; D) Celestine including dolomite with carnotite forming on celestine in remaining pores of dolomicrite; E) Celestine including dolomite and finchite; F) Smectite or illite filling pores in dolomite with carnotite; G) Disseminations of equant carnotite in dolomicrite coated with finchite and strontium carbonate; H) Equant carnotite and more bladed finchite crystals followed by strontium carbonate coating dolomite surfaces I) Detail of carnotite (brighter white mineral) and finchite filling pores in dolomite; and J) Fluorite cemented vug in dolomicrite.

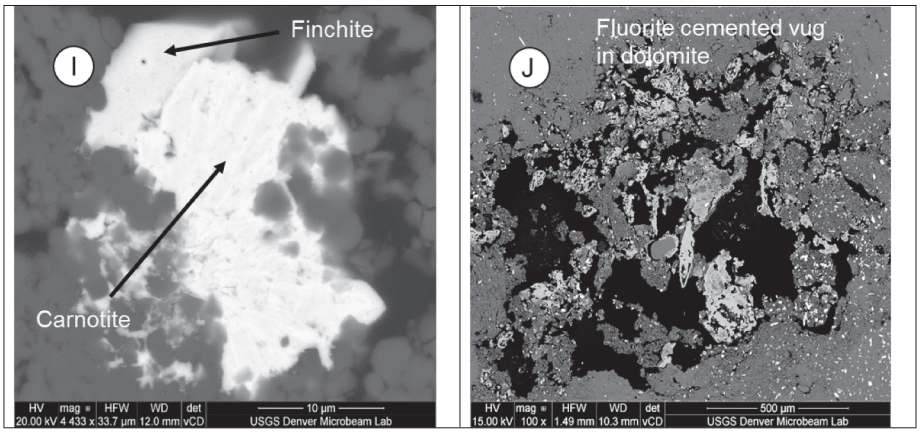


Fig. 9. (*continued*)

0.70793 for eight samples of surface water from the Pecos River to 0.70903 for five samples of groundwater from alluvial aquifers (Fig. 10b). Several groups show large variation with substantial overlap among groups. The small sample sizes for all groups included in this compilation make it impossible to estimate true population distributions for potential sources. However, $^{87}Sr/^{86}Sr$ of four groundwater samples from aquifers within the Dockum Group appear most consistent with the much narrower range of values obtained from carbonate-rich rock samples and mineralized fracture coatings measured at the Sulfur Springs Draw deposit.

3.2.3. *Uranium-series geochemistry*

The isotopic compositions of U and Th were determined in samples of the Sulfur Springs Draw deposit and adjacent carbonates to investigate uranium-disequilibrium ages of the host rock and subsequent mineralization (see Appendix A for U-series methodology). Thirteen analyses of lacustrine dolomite host rock and associated carnotite-rich fracture surfaces were analyzed from material collected from outcrop within the mineralized zone. Nine subsamples from five specimens of Pleistocene carbonate-rich material located adjacent to the Sulfur Springs Draw deposit were also analyzed, as were three analyses of a red-colored finely layered carbonate in the Pliocene Couch Member of the Ogallala Formation near the Slaton occurrence in the northern portion of the SHP (Table 4). Analytical techniques and details of sampling are summarized in Appendix A.

In the mineralized area, two samples of micritic (< 5 µm diameter) lacustrine dolomite described as non-mineralized have uranium concentrations ranging from 9.8 to 18 ppm U (SSD15-01A-1 and SSD15-01A-2) and from 54 to 96 ppm U (SSD15-01C-1 and SD15-01C-2). Both specimens are cut by fractures with minor (SSD15-01A-3) to substantial (SSD15-01C-3 and SD15-01C-4) coatings of uranium minerals. Scrapings of those fracture surfaces over small areas yield aliquots with concentrations of 3.4 to 11.3 wt% uranium (Table 4). Samples SSD15-01A-1 and SSD15-01A-2 may incorporate carnotite disseminated in dolomite (Fig. 9B); however, sampling was not precise enough to determine if carnotite was included (Appendix A). Analyses of Pleistocene carbonate-rock samples SSD15-02 to SSD15-06 collected from outside the main Sulfur Springs Draw mineralized zone contained uranium concentrations of 4.5 to 71 ppm, similar to host carbonate SSD15-01 associated with abundant U mineralization on fractures (Table 4). Samples of laminated, pink dolomite were also sampled near the Slaton occurrence in the northern SHP (Fig. 7). Three subsamples from a single hand specimen had uranium concentrations ranging from 342 to 585 ppm U (Ziel-3B-USGS-2 to 3; Table 4). Although no uranium minerals were identified in this sample, elevated uranium concentrations are highly anomalous for carbonate rock. Concentrations of uranium in unmineralized surficial carbonate elsewhere in the western United States are typically less than 15 ppm U (Fletcher et al., 2010; Paces, 2014, 2015; Paces and Whelan, 2012; Sharp et al., 2003). The median uranium content for unmineralized carbonates near the Sulfur Springs Draw deposit is 14.6 ppm U (Table 4). Fission track radiography of a polished thin section of uranium-rich sediment from near Slaton showed that uranium is associated with sparry dolomite cement and with masses of relatively pure micritic dolomite (Fig. 11).

Concentrations of Th for carbonate-rich samples are low (0.52 to 2.82 ppm Th) relative to U resulting in elevated U/Th (and $^{230}Th/^{232}Th$ activity ratios, hereafter designated using square brackets, e.g., $[^{230}Th/^{232}Th]$) values that are favorable to U-series dating. Consequently, corrections for initial ^{230}Th present at the time of carbonate formation are negligible, as are age uncertainties associated with subtraction of an unknown detrital component. The only exception is sample SSD15-03-2 consisting of micritic carbonate with a Th concentration of 18.2 ppm Th. A $^{230}Th/U$ ratio could not be calculated for this sample due to the presence of excessive amounts of ^{232}Th.

U-series isotope data for host rock and fracture minerals from sample SSD15-01 result in finite $^{230}Th/U$ ages ranging from 191 ± 4 ka to 3.81 ± 0.02 ka. Ages show a bimodal distribution with young fracture coatings (8.50 to 3.81 ka) and more ancient host rocks (191 to 15.8 ka). Initial $[^{234}U/^{238}U]$ values calculated for subsamples of SSD15-01 also show a range of values from 1.119 to 1.370 with fracture coatings having the lowest values. Host carbonate with the highest U concentrations (SSD15-01C) have lower initial $[^{234}U/^{238}U]$ values than host carbonate with lower U concentrations (SSD15-01A).

U-series ages cannot be calculated for most Pleistocene carbonate samples collected from near Sulfur Springs Draw, but outside the mineralized zone. Elevated $[^{230}Th/^{238}U]$ values in those subsamples (Table 4) reflect an excess in daughter ^{230}Th relative to amounts obtainable from in situ radioactive decay of its parent, ^{234}U. The mechanism most likely to cause this feature is post-depositional removal of U relative to Th (U-loss) due to the much greater solubility of U in near-surface geochemical environments. However, two of the nine subsamples of Pleistocene carbonate have $[^{230}Th/^{238}U]$ values that yield finite $^{230}Th/U$ ages of 121.3 ± 1.0 ka (sample SSD15-05-2) and 125.8 ± 1.1 ka (sample SSD15-06-1). Those ages are intermediate between results for host carbonate with low-U (SSD15-01A) and host carbonate with high-U (SSD15-01C). Initial $[^{234}U/^{238}U]$ values for those same subsamples are also intermediate between low- and high-U host carbonate.

The uranium-rich (342–585 ppm, Table 4) pink laminated dolomite sample collected from the Slaton area has isotopic characteristics that indicate a much older apparent age compared to carbonates from the Sulfur Springs Draw area. Both $[^{230}Th/^{238}U]$ and $[^{234}U/^{238}U]$ compositions are very close to secular equilibrium values of 1.000 (Figure A-2) indicating that (1) the dolomite remained closed to isotope exchange since it incorporated uranium, and (2) the material is very near the upper limit for the U-series dating system. Finite $^{230}Th/U$ ages

Table 4
Uranium, thorium and strontium isotope geochemistry - Southern High Plains, Texas.

Sample Name	Latitude	Longitude	Occurrence/Formation	Sample weight, g	[U], μg/g	[Th], μg/g	Measured activity ratios[a]				
							$^{232}Th/^{238}U \pm 2\sigma$		$^{230}Th/^{238}U \pm 2\sigma$		$^{234}U/^{238}U \pm 2\sigma$
Sulfur Springs Draw											
SSD15-01A-1	32.44203	−101.87003	Lacustrine carbonate/Unknown formation	0.02202	9.78	0.517	0.01742	0.00010	1.042	0.0044	1.214
SSD15-01A-1a	32.44203	−101.87003	Lacustrine carbonate/Unknown formation	0.01110	10.7	0.53	0.01635	0.00011	0.994	0.0078	1.210
SSD15-01A-2	32.44203	−101.87003	Lacustrine carbonate/Unknown formation	0.02883	17.8	0.569	0.01056	0.00006	1.007	0.0045	1.205
SSD15-01A-2a	32.44203	−101.87003	Lacustrine carbonate/Unknown formation	0.02770	14.2	0.553	0.01283	0.00008	1.041	0.0066	1.210
SSD15-01A-3	32.44203	−101.87003	Ore on fracture surface/Unknown formation	0.00339	11,300	1.84	0.00005	0.00000	0.056	0.0002	1.180
SSD15-01C-1	32.44203	−101.87003	Lacustrine carbonate/Unknown formation	0.02273	61.2	0.557	0.00300	0.00002	0.176	0.0007	1.132
SSD15-01C-1a	32.44203	−101.87003	Lacustrine carbonate/Unknown formation	0.01053	96.4	1.25	0.00429	0.00003	0.156	0.0010	1.133
SSD15-01C-2	32.44203	−101.87003	Lacustrine carbonate/Unknown formation	0.02932	65.8	0.589	0.00295	0.00002	0.198	0.0010	1.135
SSD15-01C-2a	32.44203	−101.87003	Lacustrine carbonate/Unknown formation	0.02006	53.8	0.557	0.00341	0.00002	0.224	0.0018	1.143
SSD15-01C-3	32.44203	−101.87003	Ore on fracture surface/Unknown formation	0.00088	56,200	0.974	0.00001	0.00000	0.084	0.0004	1.124
SSD15-01C-3a	32.44203	−101.87003	Ore on fracture surface/Unknown formation	0.00223	56,800	1.16	0.00001	0.00000	0.062	0.0003	1.130
SSD15-01C-4	32.44203	−101.87003	Ore on fracture surface/Unknown formation	0.00078	84,100	1.71	0.00001	0.00000	0.051	0.0003	1.117
SSD15-01C-4a	32.44203	−101.87003	Ore on fracture surface/Unknown formation	0.00206	34,200	1.56	0.00002	0.00000	0.039	0.0002	1.127
SSD15-02–1	32.45497	−101.86478	Carbonate breccia/Tule Formation	0.00562	71.1	2.08	0.00957	0.00007	9.437	0.0382	1.264
SSD15-02–2	32.45497	−101.86478	Carbonate breccia/Tule Formation	0.02243	10.4	2.77	0.08740	0.00050	16.319	0.0652	1.547
SSD15-03–1	32.45472	−101.86467	Micritic carbonate/Tule Formation	0.02243	6.75	1.89	0.09208	0.00054	13.722	0.0532	1.280
SSD15-03–2	32.45472	−101.86467	Micritic carbonate/Tule Formation	0.01660	4.5	18.2	1.33353	0.01105	1.033	0.0128	0.999
SSD15-04–1	32.45244	−101.86386	Cemented ash/Tule Formation	0.02219	10.3	2.41	0.07736	0.00048	2.129	0.0089	1.204
SSD15-05–1	32.45028	−101.86478	Micritic carbonate/Tule Formation	0.02102	9.76	2.82	0.09514	0.00060	2.879	0.0163	1.212
SSD15-05–2	32.45028	−101.86478	Micritic carbonate/Tule Formation	0.03277	58.3	0.815	0.00460	0.00003	0.832	0.0033	1.206
SSD15-06–1	32.44569	−101.86836	Carbonate tufa/Unknown formation	0.01865	55.6	0.815	0.00482	0.00003	0.850	0.0033	1.207
SSD15-06–2	32.44569	−101.86836	Carbonate tufa/Unknown formation	0.00735	6.93	0.922	0.04377	0.00028	6.728	0.0326	2.483
Slaton Occurrence											
Ziel-3B-USGS-1	33.44344	−101.53628	Banded dolomite/Couch Member	0.00104	585	0.541	0.000299	0.000025	1.008	0.0039	1.006
Ziel-3B-USGS-2	33.44344	−101.53628	Banded dolomite/Couch Member	0.00087	350	0.537	0.000500	0.000050	1.004	0.0040	1.008
Ziel-3B-USGS-3	33.44344	−101.53628	Banded dolomite/CouchMember	0.00103	342	0.592	0.000566	0.000043	1.008	0.0039	1.004

Sample Name	Measured activity ratios[a]		Detritus-corrected activity ratios[b]					$^{230}Th/U$ Age (ka)[d] ± 2σ		Initial $^{234}U/^{238}U$ AR[d] ± 2σ		$^{87}Sr/^{86}Sr$[e] ± 2σ	
	$^{234}U/^{238}U \pm 2\sigma$	$^{230}Th/^{232}Th$	$^{230}Th/^{238}U \pm 2\sigma$		$^{234}U/^{238}U \pm 2\sigma$		$\rho_{48\text{-}08}$[c]						
Sulfur Springs Draw													
SSD15-01A-1	0.0026	59.8	1.0428	0.0057	1.2166	0.0033	0.024	189.4	2.9	1.370	0.005	—	—
SSD15-01A-1a	0.0029	60.8	0.9938	0.0085	1.2125	0.0035	−0.002	170.6	3.5	1.344	0.005	0.708504	0.000010
SSD15-01A-2	0.0026	95.4	1.0067	0.0050	1.2067	0.0029	0.002	178.	2.4	1.342	0.004	—	—
SSD15-01A-2a	0.0027	81.2	1.0415	0.0072	1.2118	0.0031	0.010	191.	3.6	1.363	0.005	0.708511	0.000010
SSD15-01A-3	0.0030	1057	0.0560	0.0003	1.1796	0.0030	0.000	5.3	0.03	1.182	0.003	0.708505	0.000009
SSD15-01C-1	0.0024	58.9	0.1745	0.0014	1.1323	0.0024	−0.046	18.2	0.2	1.139	0.003	—	—
SSD15-01C-1a	0.0024	36.3	0.1529	0.0019	1.1338	0.0024	−0.068	15.8	0.2	1.140	0.003	0.708496	0.000009
SSD15-01C-2	0.0025	67.0	0.1958	0.0015	1.1352	0.0025	−0.040	20.6	0.2	1.143	0.003	—	—
SSD15-01C-2a	0.0043	65.7	0.2217	0.0022	1.1431	0.0043	−0.021	23.4	0.3	1.153	0.005	0.708494	0.000009
SSD15-01C-3	0.0029	16,044	0.0843	0.0004	1.1236	0.0029	0.000	8.5	0.05	1.127	0.003	—	—
SSD15-01C-3a	0.0033	9606	0.0617	0.0003	1.1299	0.0033	0.000	6.1	0.03	1.132	0.003	0.708498	0.000010
SSD15-01C-4	0.0028	7984	0.0512	0.0003	1.1170	0.0028	0.000	5.1	0.03	1.119	0.003	—	—
SSD15-01C-4a	0.0032	2616	0.0388	0.0002	1.1274	0.0032	0.000	3.8	0.02	1.129	0.003	0.708479	0.000008
SSD15-02–1	0.0033	986	9.501	0.050	1.2664	0.0036	0.180	Excess 230Th		Not Calculated		0.708543	0.000009
SSD15-02–2	0.0033	187	17.45	0.61	1.5876	0.0231	0.929	Excess 230Th		Not Calculated		0.708568	0.000008
SSD15-03–1	0.0034	149	14.71	0.54	1.3018	0.0145	0.802	Excess 230Th		Not Calculated		0.708604	0.000008
SSD15-03–2	0.0024	0.8	0.27	10.30	1.0152	2.3252	−0.063	Excessive 232Th		Not Calculated		0.708586	0.000010

(*continued on next page*)

Table 4 (*continued*)

Sample Name	Measured activity ratios[a]		Detritus-corrected activity ratios[b]				^{230}Th/U Age (ka)[d] ± 2σ		Initial ^{234}U/^{238}U AR[d] ± 2σ		^{87}Sr/^{86}Sr[e] ± 2σ	
	^{234}U/^{238}U ± 2σ	^{230}Th/^{232}Th	^{230}Th/^{238}U ± 2σ		^{234}U/^{238}U ± 2σ		$\rho_{48\text{-}08}$[c]					
SSD15-04–1	0.0031	27.5	2.2016	0.0430	1.2168	0.0101	0.626	Excess 230Th		Not Calculated		0.70856	0.000010
SSD15-05–1	0.0036	30.3	3.0305	0.0861	1.2292	0.0129	0.683	Excess 230Th		Not Calculated		0.708542	0.000010
SSD15-05–2	0.0025	181	0.8314	0.0034	1.2065	0.0026	−0.013	121.3	1.0	1.291	0.003	0.708518	0.000010
SSD15-06–1	0.0025	176	0.8494	0.0035	1.2076	0.0026	−0.012	125.8	1.1	1.296	0.003	0.708516	0.000010
SSD15-06–2	0.0094	154	6.9316	0.1110	2.5355	0.0292	0.887	Excess 230Th		Not Calculated		0.708516	0.000011
Slaton Occurrence													
Ziel-3B-USGS-1	0.0022	3372	1.0079	0.0039	1.0064	0.0022	0.00000	695	+290 −140	1.049	+0.049 −0.017	—	—
Ziel-3B-USGS-2	0.0024	2006	1.0035	0.0040	1.0078	0.0024	0.00000	542	+110 −65	1.036	+0.010 −0.008	—	—
Ziel-3B-USGS-3	0.0021	1781	1.0077	0.0039	1.0040	0.0021	0.00000	761	+2080 −160	1.043	+0.044 −0.019	—	—

[a] Measured isotope ratios corrected for mass fractionation, spike contributions, procedural blank and normalized relative to a standard value for NIST SRM 4321b ^{234}U/^{238}U = 0.0000529. Atomic ratios converted to activity ratios using published decay constants (Steiger and Jäger, 1977; Cheng et al., 2013)

[b] Corrected activity ratios based on measured ^{232}Th/^{238}U assuming the ^{232}Th-bearing detrital component has an atomic Th/U of 4 and activity ratios and 2σ errors: ^{232}Th/^{238}U = 1.276 ± 0.64; ^{234}U/^{238}U = 1.0 ± 0.1; and ^{230}Th/^{238}U = 1.0 ± 0.25.

[c] $\rho_{48\text{-}08}$ = error correlation between ^{234}U/^{238}U and ^{230}Th/^{238}U activity ratios.

[d] ^{230}Th/U age, initial ^{234}U/^{238}U activity ratio (AR) and associated errors calculated using Detritus-Corrected activity ratios

[e] Atomic ratio normalized relative to the accepted value for NIST SRM 987 ^{87}Sr/^{86}Sr = 0.710248 (McArthur et al., 2001).

calculated using a Monte Carlo approach with solutions constrained to runs yielding positive ages (Ludwig, 2012) result in age estimates between $761^{+280}/_{-160}$ ka and $542^{+110}/_{-65}$ ka (Table 4). These dates are substantially older than the upper limit commonly used for the U-series dating range (~5 times the 75,690-year half-life for ^{230}Th), and it is likely the material is older than values reported here. Initial [^{234}U/^{238}U] of 1.036 to 1.049 reported in Table 4 are interpreted as artefacts of the compositions being so close to secular equilibrium and likely underestimate the original values.

Results of isotope analyses for samples from the mineralized portion of the Sulfur Springs Draw deposit do not follow U-series isotope evolution curves and cannot be explained by closed-system radioactive decay from a single fluid source. Isotopic evolution of [^{234}U/^{238}U] and [^{230}Th/^{238}U] under closed-system conditions where the only process affecting ratios is the radioactive decay of ^{234}U and ingrowth of ^{230}Th, results in compositions that follow paths similar to the heavy curved lines in Fig. 12 starting at the initial value of [^{234}U/^{238}U] present in the source water at time 0 (that is, when [^{230}Th/^{238}U] = 0.0). Instead of following these trajectories, data for samples of SSD15-01A and SSD15-01C form positively sloped linear arrays that cross evolution curves at high angles. In contrast, open-system processes involving gains or losses of material are expected to result in subhorizontal arrays where ^{230}Th/^{238}U AR values vary widely due to the greater mobility of uranium relative to thorium while [^{234}U/^{238}U] remains relatively unaffected (heavy arrow labeled U loss in Fig. 12).

Data for Sulfur Spring Draw host rock and fracture coatings show trends that are best interpreted as binary mixing curves between two end members (Fig. 13). The older end member is represented by low-U, lacustrine carbonate formed at least 190,000 years ago from solutions with [^{234}U/^{238}U] somewhat > 1.37. This composition is commonly observed in soil water and surface water in the western United States and is consistent with a lacustrine setting fed by streamflow during wetter climate conditions in the middle Pleistocene. The younger end member is represented by U-rich, carnotite deposits on fracture surfaces mobilized between ~8.5 and ~3.8 ka, or more recently. The younger, U-rich solutions had substantially lower [^{234}U/^{238}U] values (< 1.13) than water from which the lacustrine carbonate precipitated and requires a different fluid source. Mineralizing solutions infiltrated into the matrix of the host rock to varying degrees—more so in the carbonate sample hosting extensive fracture mineralization (SSD15-01C), and less so for the carbonate hosting only minor fracture mineralization (SSD15-01A). Two samples from outside the mineralized zone that yielded finite age estimates (SSD15-05-2 and SSD15-06-1) have compositions and ages that are also intermediate between values for unmineralized and mineralized carbonate host of SSD15-01. Those samples plot along a binary mixing curve connecting unmineralized host carbonate SSD15-01A and the one sample of carnotite fracture scraping from the same sample (upper curve in Fig. 13). Both samples have elevated U concentrations (56–58 ppm) and were presumably affected by U-rich fluids introduced as part of the same process affecting more highly mineralized samples of SSD15-01. Differences between [^{234}U/^{238}U] values for fracture minerals from SSD15-01A and SD15-01C imply that solutions responsible for U mineralization may have had multiple sources or pathways leading to the sites of deposition.

In summary, U-series ages obtained for near-surface materials from the Sulfur Springs Draw deposit are interpreted as defining two significant episodes in the region: (1) the timing of lacustrine carbonate formation in Pleistocene lakes around 190 ka or older, and (2) introduction of U-bearing solutions during the Holocene between about 9 and 3 ka (Fig. 13). The younger ages span a period of aeolian activity in the SHP (Holliday, 1985; Rich, 2013) and may record a more arid period with greater rates of evaporation that drove increased upward migration of solutions in the shallow unconfined aquifer. Intermediate ages calculated for individual samples listed in Table 4 are interpreted as mixtures of older and younger components that do not represent actual geologic events intermediate between those two episodes.

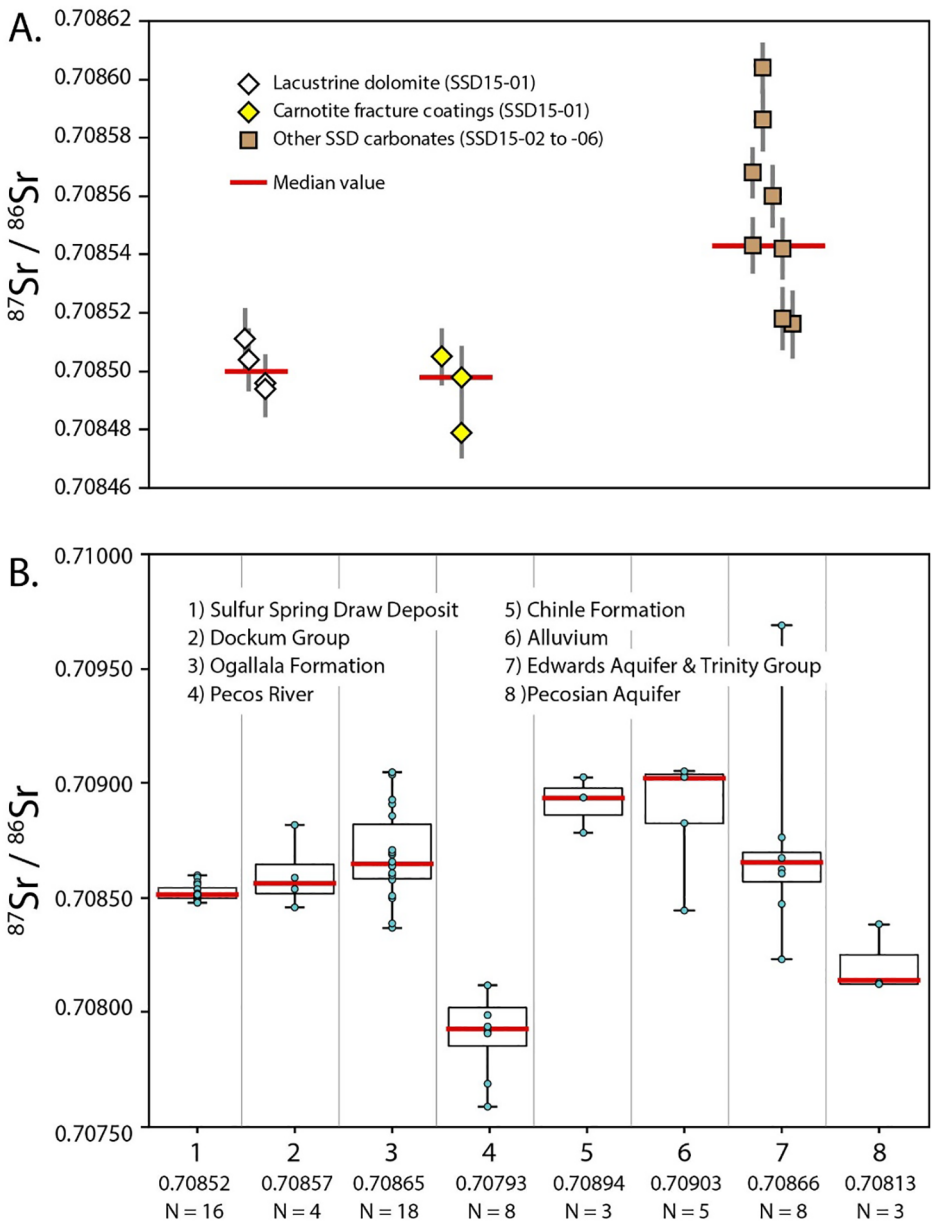


Fig. 10. $^{87}Sr/^{86}Sr$ compositions for (A) host rock and mineralized fracture coatings from the Sulfur Springs Draw (SSD) deposits and adjacent carbonates, and (B) rock and mineral samples shown in A compared to values in groundwater and surface water samples from regional aquifers and streams. Data points shown in A are from Table 4 and include individual analytical error bars. Data points shown in B are from Table 5 along with statistical limits including the first and third quartiles (boxes), medians (red lines and values given at the bottom of the plot along with the number of analyses included in the group), and total range (whiskers). (For interpretation of the references to color in this figure legend, the reader is referred to the web version of this article.)

Alternatively, the younger ages determined from carnotite-rich surface scrapings may reflect a more-or-less continuous history of uranium mobility in the near-surface environment rather than a discrete introduction of U-bearing fluids. However, if those conditions prevailed, U would likely be dissolved and reprecipitated whereas Th would remain immobile resulting in material with unsupported ^{230}Th. The consequences of this type of behavior are apparent for some carbonate samples outside the main Sulfur Springs Draw ore body, but not for lower-U lacustrine carbonates representing the mineralized host. Therefore, we prefer an interpretation involving the geologically recent introduction of U-rich fluids, even if they are associated with a mobilization event that redistributed earlier-formed materials.

Holocene-aged uranium mineralization introduced into Sulfur Spring Draw carbonates as well as elevated U concentrations in more ancient carbonate from the Slaton area indicates that there have been groundwater or surface water systems with substantial amounts of dissolved uranium in the SHP from at least the middle Pleistocene to Recent. Younger ages and variable initial $^{234}U/^{238}U$ measured from SSD15-01 fracture coatings may indicate that uranium minerals formed and (or) were redistributed in multiple episodes, and that the source of uranium in mineralizing fluids was distinct from surface water associated with Pleistocene lakes.

Materials available for this study were limited to surface samples collected from scattered outcrops. The only information available about buried portions of the deposits in the region is from subsurface samples that had an average uranium isotopic composition reported near secular equilibrium implying an age of roughly 1 million years or older (Waechter, 1976), consistent with results from the pink dolomite sampled near Slaton. Although mineralization age is not available for most calcrete uranium deposits, the ages estimated for Sulfur Springs Draw are similar to the 700 to 25 ka range reported for deposits in Australia (Toens, 1984).

4. Mineral systems model

4.1. Uranium and vanadium source

Two potential source rocks for uranium are identified in the region: (1) Triassic and older sediments that underlie the SHP, and (2) volcanic ash interbedded in Pleistocene rocks. Vanadium is probably derived

Table 5
Strontium isotope ratios and concentration measured from groundwater in the SHP region (National Water Information System, 2017).

National Water Information System Location Identifier	Sample Type	Sample Aquifer	$^{87}Sr/^{86}Sr$ (per mil)	Sr concentration (ppb)	Latitude	Longitude
USGS-341720103494701	Groundwater	Alluvium, Bolson Deposits and Other Surface Deposits	0.70845	1300	34.2898	−103.832975
USGS-341820103442601	Groundwater	Alluvium, Bolson Deposits and Other Surface Deposits	0.70883	1900	34.30385	−103.7397778
USGS-341954103503101	Groundwater	Alluvium, Bolson Deposits and Other Surface Deposits	0.70903	2400	34.2438222	−103.8418167
USGS-342031103464701	Groundwater	Alluvium, Bolson Deposits and Other Surface Deposits	0.70905	1100	34.3437056	−103.78265
USGS-342046103503501	Groundwater	Alluvium, Bolson Deposits and Other Surface Deposits	0.70906	1100	34.347275	−103.8453944
USGS-311323102435200	Groundwater	Artesian Well - no aquifer identified	0.70711	34,300	31.2230833	−102.731
USGS-311418102432601	Groundwater	Artesian Well - no aquifer identified	0.70764	10,400	31.2383333	−102.7238889
USGS-311422102555101	Groundwater	Capitan Reef Complex and Associated Limestones	0.70751	10,200	31.2397389	−102.9309694
USGS-341714103442502	Groundwater	Chinle Formation	0.70879	9,700	34.287425	−103.7406028
USGS-342045103442602	Groundwater	Chinle Formation	0.70894	730	34.3459194	−103.7407694
USGS-342023103493403	Groundwater	Chinle Formation	0.70903	28,000	34.3398417	−103.8262083
USGS-311610103050901	Groundwater	Dockum Group	0.70846	2800	31.2695856	−103.086828
USGS-310949103090401	Groundwater	Dockum Group	0.70854	1350	31.1634111	−103.1510306
USGS-331316102195401	Groundwater	Dockum Group	0.70859	2170	33.2211111	−102.3316889
USGS-330036102071701	Groundwater	Dockum Group	0.70882	6770	33.0101111	−102.1212806
USGS-310136102311601	Groundwater	Edwards and Associated Limestones, and Trinity Group	0.70824	8790	31.0267	−102.5210194
USGS-310718102484801	Groundwater	Edwards and Associated Limestones, and Trinity Group	0.70848	10,300	31.1216194	−102.8135389
USGS-311235103000901	Groundwater	Edwards and Associated Limestones, and Trinity Group	0.70861	3070	31.2097389	−103.0026194
USGS-330618102190801	Groundwater	Edwards and Associated Limestones, and Trinity Group	0.70863	398	33.1049889	−102.3189806
USGS-332014102100101	Groundwater	Edwards and Associated Limestones, and Trinity Group	0.70868	4280	33.33715	−102.1669806
USGS-331029102272001	Groundwater	Edwards and Associated Limestones, and Trinity Group	0.70868	3,970	33.1748611	−102.4554194
USGS-331646102220901	Groundwater	Edwards and Associated Limestones, and Trinity Group	0.70877	3570	33.2793194	−102.3691389
USGS-331045102133901	Groundwater	Edwards and Associated Limestones, and Trinity Group	0.70969	4510	33.1791667	−102.2275
USGS-330339102235001	Groundwater	Ogallala Formation	0.70837	2370	33.0607611	−102.3972306
USGS-330751102351501	Groundwater	Ogallala Formation	0.70839	4,520	33.1307389	−102.5874194
USGS-330852102130401	Groundwater	Ogallala Formation	0.7085	6120	33.1478694	−102.2176694
USGS-331755102211401	Groundwater	Ogallala Formation	0.70851	2380	33.2986111	−102.3538889
USGS-331657102131801	Groundwater	Ogallala Formation	0.70858	2590	33.2824889	−102.2216806
USGS-330351102130301	Groundwater	Ogallala Formation	0.7086	4290	33.0642389	−102.2175389
USGS-330624102091701	Groundwater	Ogallala Formation	0.7086	3100	33.10675	−102.1547306
USGS-330129102180701	Groundwater	Ogallala Formation	0.70861	3860	33.0247222	−102.3019444
USGS-331359102351201	Groundwater	Ogallala Formation	0.70864	6050	33.2330528	−102.5866667
USGS-331131102133701	Groundwater	Ogallala Formation	0.70866	4800	33.1919444	−102.2269444
USGS-341640103470501	Groundwater	Ogallala Formation	0.70869	4000	34.2781778	−103.78535
USGS-341743103470801	Groundwater	Ogallala Formation	0.7087	5800	34.2953333	−103.7859528
USGS-341825103470301	Groundwater	Ogallala Formation	0.70871	16,000	34.3070694	−103.7848611
USGS-341958103485401	Groundwater	Ogallala Formation	0.70886	1,700	34.3328667	−103.8153917
USGS-342048103492701	Groundwater	Ogallala Formation	0.70891	840	34.3467556	−103.8249139
USGS-342152103444201	Groundwater	Ogallala Formation	0.70893	910	34.3638361	−103.7457278
USGS-342023103493401	Groundwater	Ogallala Formation	0.70904	990	34.339775	−103.8262667
USGS-342045103442601	Groundwater	Ogallala Formation	0.70905	3600	34.3459194	−103.7407694
USGS-311402102285400	Surface Water	Pecos River	0.70759	14,400	31.2338889	−102.4816944
USGS-311557102355600	Surface Water	Pecos River	0.70769	15,500	31.2658056	−102.599
USGS-311820102523900	Surface Water	Pecos River	0.70791	13,500	31.3055278	−102.8774722
USGS-313256103294600	Surface Water	Pecos River	0.70792	13,500	31.5487778	−103.4960278
USGS-08412500	Surface Water	Pecos River	0.70794	14,700	31.8726265	−103.8315824
USGS-08437710	Surface Water	Pecos River	0.70799	14,800	31.3668055	−103.0059908
USGS-08446550	Surface Water	Pecos River	0.70812	15,600	31.0793611	−102.3603611
USGS-310204102131500	Surface Water	Pecos River	0.70812	14,600	31.0344722	−102.2209722
USGS-311602102400901	Groundwater	Pecosian Series (Pliocene Section of Llano Estacado Sands)	0.70813	15,000	31.2693389	−102.6821389
USGS-311602102400601	Groundwater	Pecosian Series (Pliocene Section of Llano Estacado Sands)	0.70813	12,300	31.2694194	−102.6760889
USGS-310625103175201	Groundwater	Pecosian Series (Pliocene Section of Llano Estacado Sands)	0.70839	1300	31.10685	−103.2977694
USGS-310806103171901	Groundwater	Rustler Formation	0.70763	3390	31.1350194	−103.2879611
USGS-315300103550900	Surface Water	Salt Creek	0.70759	20,400	31.8832222	−103.9190833
USGS-08446600	Groundwater	Spring - no aquifer identified	0.70925	8970	31.0019	−102.9235833
USGS-08437000	Groundwater	Spring - no aquifer identified	0.7097	9060	31.2674333	−102.9582833

(*continued on next page*)

Table 5 (*continued*)

National Water Information System Location Identifier	Sample Type	Sample Aquifer	$^{87}Sr/^{86}Sr$ (per mil)	Sr concentration (ppb)	Latitude	Longitude
USGS-332054102262101	Groundwater	Unknown	0.70856	2100	33.3483333	−102.4391667
USGS-331305102122401	Groundwater	Unknown	0.70856	6840	33.2180556	−102.2066667
USGS-325731102311201	Groundwater	Unknown	0.70867	4800	32.9586111	−102.52
USGS-330904102292501	Groundwater	Unknown	0.70869	7150	33.1511111	−102.4902778

from clay, mafic minerals and iron oxides in Triassic rocks.

4.1.1. Triassic and older source rock

The Upper Triassic Dockum Group, along with the laterally equivalent Chinle Formation, as well as Permian and Pennsylvanian strata underlying the SHP have been targeted for uranium exploration by private industry and evaluated by the U.S. government (Amaral, 1979; Carlisle, 1978; Finch, 1972, 1975; Hill et al., 2009; McGowen et al., 1981; Seni et al., 1980). Geochemical (uranium concentration) and geophysical (radiometric) anomalies in well logs have been identified in the Dockum Group and Chinle Formation in Texas (Fig. 14). Samples collected from 93 localities of Dockum Group along the eastern escarpment of the SHP demonstrate that lacustrine facies contain up to 700 ppm U and channel lag deposits contain up to 63 ppm U (McGowen et al., 1977). Where uranium content is high in the Dockum, the vanadium content is commonly also elevated (McGowen et al., 1981). Gamma anomalies in subsurface drill logs are another line of evidence that uranium is heterogeneously enriched in portions of the Dockum (Bradley and Kalaswad, 2003) (Fig. 14).

Uranium occurrences are described in Dockum Group and equivalent sedimentary rocks where they crop out along the northern and eastern escarpments of the SHP, and in the Pecos River valley (Finch, 1975). Anomalous uranium is found in grayish and greenish rock and carbonaceous material, silicified wood and cuprous spherules and nodules, most commonly in ancient channels where organic debris accumulated. Ore is urano-organic compounds with secondary tyuyamunite, meta-tyuyamunite, autunite, bayleyite, liebigite and cuprosklodowskite.

Uranium with associated vanadium (up to 1000 ppm V) is hosted in the Dockum Group where it is exposed along the margins of the SHP (Fig. 14; Finch, 1975). About 700 tonnes of ore was mined from the Post district southeast of Lubbock, and an additional 10 tonnes from the Rattlesnake mine in Briscoe County, both containing an average of about 170 ppm U (Fig. 14; Finch, 1975).

Potential source rocks are also identified in units underlying the Dockum Group. Uranium deposits are hosted in the Permian Cutler Formation, Coconino Sandstone, and Hermit Formation and in the Pennsylvanian Supai Group in the Colorado Plateau. Rocks of Permian age were evaluated for potential uranium deposits in the SHP region (Campbell and Steele, 1976). Uranium-bearing asphaltite sourced from Permian and Pennsylvanian age rocks is described in the northern portion of the SHP and may provide an additional source of uranium in the region (Pierce et al., 1964).

Concentrations of uranium and vanadium within Triassic rock can become a uranium and vanadium source by changes in oxidation and the flow of fluid through these rocks. Changes in basin tectonics (uplift, faulting, and folding), as well as erosion and evolving topography that bring U-bearing reduced facies into contact with oxygenated groundwater or surface water can remobilize uranium. In the SHP, dissection and exposure following regional uplift may have rejuvenated the flow of groundwater through the Dockum, mobilizing uranium and vanadium into groundwater and making it available as a metal source.

Differences in $^{87}Sr/^{86}Sr$ measured from solid samples collected in and adjacent to the Sulfur Springs Draw deposit compared to those from groundwater and surface water in the SHP are small, but statistically significant. Strontium isotopes measured from the Sulfur Springs Draw

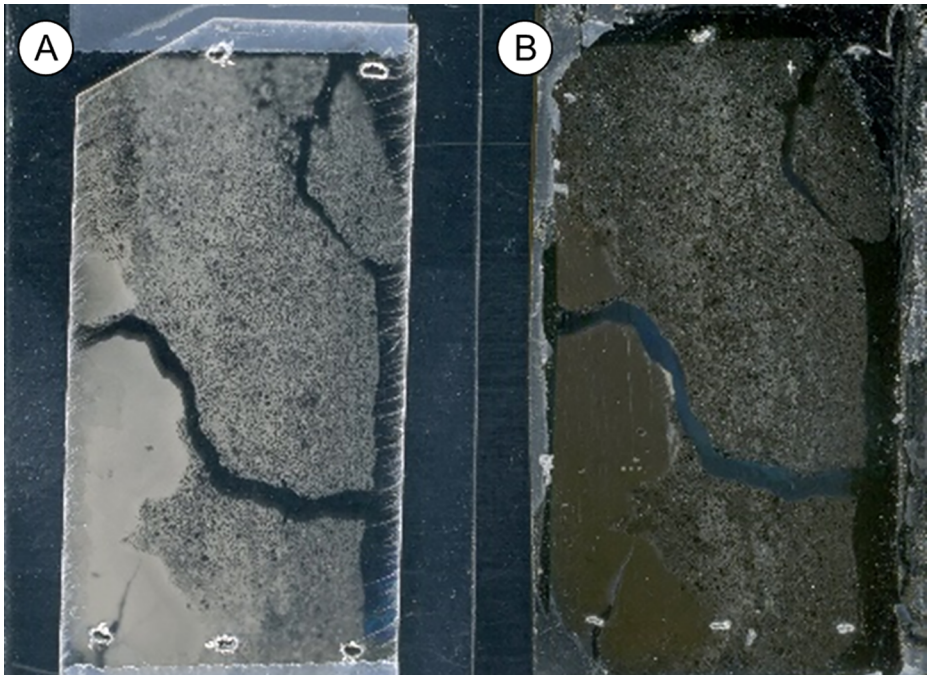


Fig. 11. Fission track radiograph (A) of a thin section of dolomite-bearing sediment (B) collected from the Slaton area. The lighter colored areas in (A) indicate areas of greatest fission track density and therefore highest uranium concentration. Uranium is concentrated in sparry dolomite that cements siliclastic grains and in a mass of finer grained micritic dolomite shown in the lower left portion of the thin section. Thin sections are each 26 mm × 44 mm.

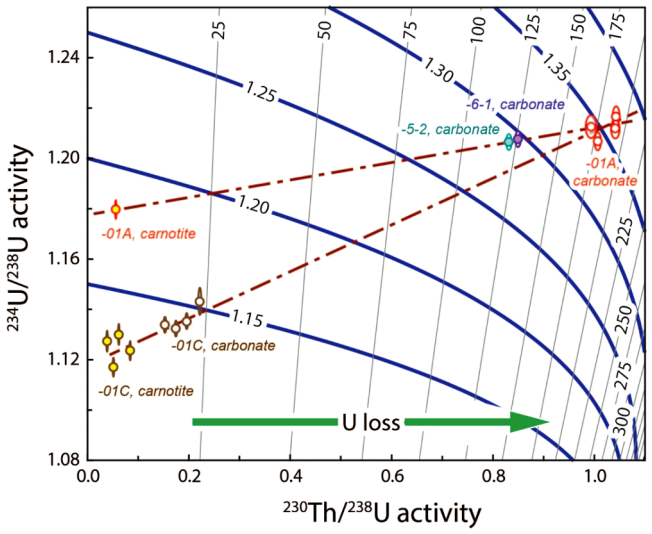


Fig. 12. U-series isotope evolution diagram showing $^{234}U/^{238}U$ and $^{230}Th/^{238}U$ activity ratios for samples collected from the Sulfur Springs Draw area. Straight light lines are isochrons labeled in thousands of years before present. Curved heavy lines show the foci of isotope compositions resulting from radioactive decay and ingrowth starting from different values for the initial $^{234}U/^{238}U$ activities. Data are shown as symbols overlying 2-sigma error ellipses. Thick arrow shows the expected displacement of compositions produced by the loss of U from the system. Dash-dot lines represent trends expected for binary mixing of older and younger components.

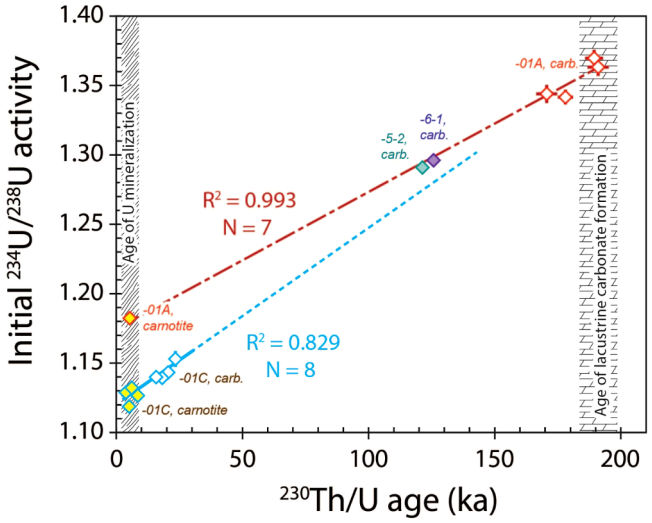


Fig. 13. $^{234}U/^{238}U$ activity ratio v. $^{230}Th/U$ in thousands of years before present (ka) for samples collected from the Sulfur Springs Draw area.

deposit appear most consistent with strontium isotope signatures observed in groundwater from the Dockum Group aquifer (Tables 4, 5; Fig. 10b). The presence of Sr in mineralizing solutions with $^{87}Sr/^{86}Sr$ compositions derived from a Dockum groundwater source implies that Dockum sediments were also the likely source of uranium for Sulfur Springs Draw deposits and, by analogy, for other uranium occurrences throughout the SHP. Similar $^{87}Sr/^{86}Sr$ values in mineralized and unmineralized carbonate in the Sulfur Springs Draw area also suggest that Dockum aquifer discharge may have supplied water to Pleistocene lakes in the region.

4.1.2. Volcanic ash source rock

Volcanic ash collected near Sulfur Springs Draw contains 6.9 ppm uranium, and ash near Slaton, Texas in the northern portion of the SHP contains 7.2 ppm uranium (Van Gosen and Hall, 2017). Those concentrations are consistent with uranium in silicic rocks (Rogers and Adams, 1978). Furthermore, ash has commonly been implicated as a source of uranium in other regions (Zielinski, 1983). Ash in the SHP forms discontinuous lenses and thin layers and is not volumetrically significant, challenging the hypothesis that this material is an important source of uranium. However, ash may be more abundant throughout the region than currently recognized because of the sparse exposures in the SHP and the difficulty in distinguishing ash from other fine-grained siliciclastic rocks in outcrop.

4.2. Transport

Known uranium occurrences largely cluster along modern channel systems in the SHP, implying spatial control on the location of calcrete uranium deposits (Fig. 7). Northwest- to southeast-trending drainage systems developed first on an erosional surface developed on Cretaceous rocks in the SHP, and these drainage patterns exist today. It is possible that deposits have been identified thus far in drainages because that is where they are best exposed. However, exploration using airborne gamma surveys, gamma well-logs from oil and gas wells in the region, groundwater sampling, and drilling of hundreds of holes in the SHP has been directed at locating concealed deposits. Because these methods did not identify substantial prospects in the subsurface, the location of known occurrences in drainages is thought to be a first-order control on mineralization, and not just the result of better exposure.

Modern groundwater in the SHP contains concentrations of vanadium that range from 20 to 150 µg/L and uranium from 2 to 30 µg/L. The highest concentrations of dissolved uranium and vanadium tend to occur in the southern and eastern portions of the region (Ranalli and Yager, 2016; Reedy et al., 2011). Uranium has been variably elevated in groundwater and (or) surface water in the SHP from at least the Pleistocene to Recent time. Evidence for this highly U-anomalous water is the dolomite collected from the Couch Member near Slaton, and uraniferous opal within the Ogallala Formation reported from the Plainview quadrangle–both in the northern portion of the SHP (Table 4; Amaral, 1979).

Uranium distribution in the Dockum Group, is likely related to different rates of groundwater transport in this geologic unit. In the lower, sandier Dockum, uranium concentrations measured by gamma anomalies in oil well logs are more prevalent in the eastern portion of the unit (yellow polygons in Fig. 14). In the less sandy, upper Dockum, where groundwater would less effectively transport uranium, concentrations measured by gamma anomalies in oil well logs remain in the central portion of the unit (orange polygon in Fig. 14) (McGowen et al., 1977). Portions of the Dockum where groundwater recharge rates are higher, such as in the southwestern SHP, do not show subsurface gamma anomalies (McGowen et al., 1977), possibly indicating that uranium was flushed from these areas.

Water in the Dockum moves downward into the underlying Permian sequence in the northern portion of the SHP (Palo Duro Basin) (Bradley and Kalaswad, 2003; Scanlon et al., 2012); this may be a factor in explaining the lack of deposits in the northern portion of the basin because here the source and host rocks are not connected by groundwater flow. In the southern portion of the SHP, recharge moves upward from underlying Permian aquifers, through the Dockum and into overlying Cretaceous units and the Ogallala Formation (Fig. 15) (Bradley and Kalaswad, 2003; Scanlon et al., 2012). Known deposits are found where the rocks of the Dockum Group directly underlie the host Pleistocene carbonates. Thus, transport of uranium and (or) vanadium leached from the Dockum strata would be direct, as exemplified by the Sulfur Springs Draw and Buzzard Draw deposits in Martin County (Fig. 6).

Calcrete uranium occurrences identified in the SHP are found near modern ephemeral lakes and along drainages where higher rates of groundwater discharge and evaporation are likely to occur (Waechter, 1974), particularly where the depth to groundwater, measured before

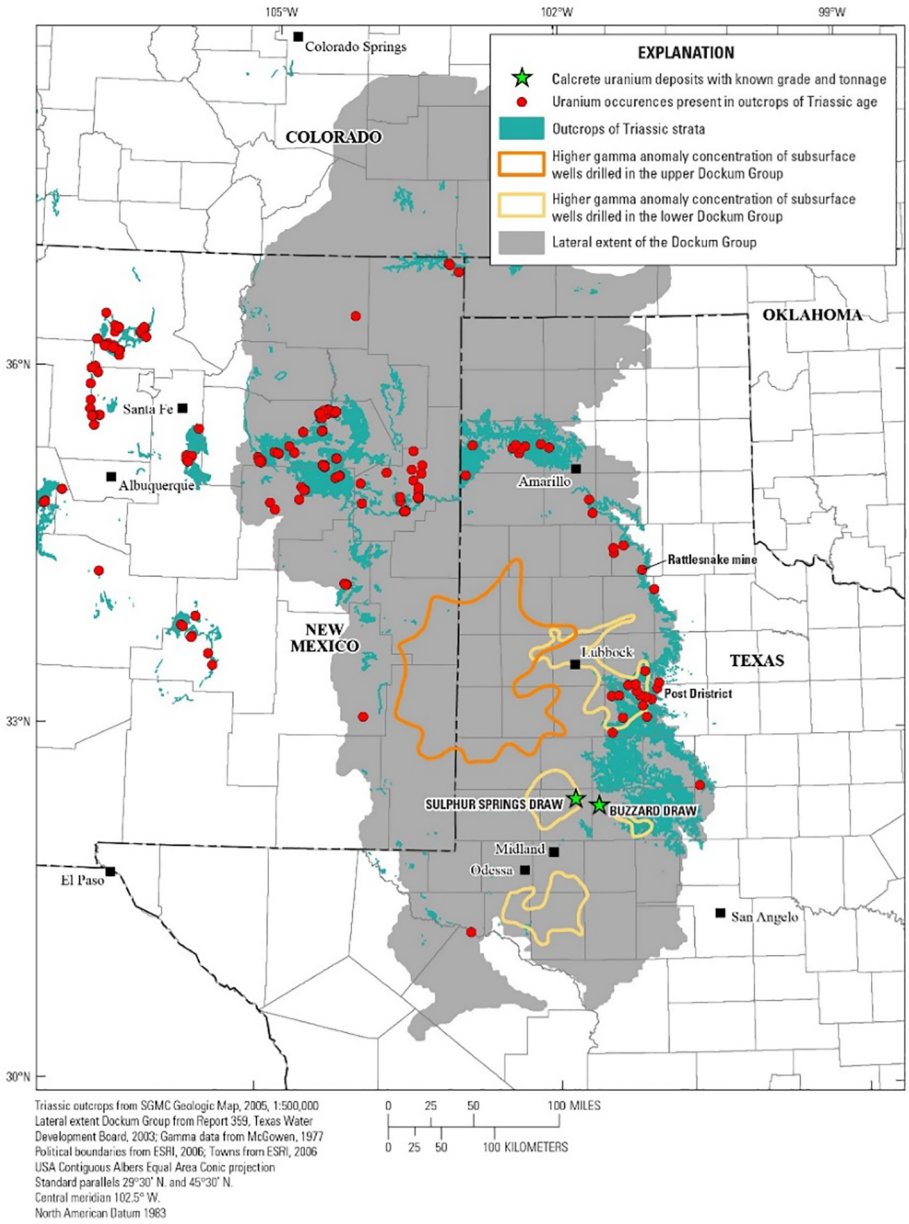


Fig. 14. Extent of the Dockum Group, location of uranium occurrences in the Dockum Group and Chinle Formation, and region of high gamma anomalies in the upper and lower parts of the Dockum (Finch, 1975; McGowen, 1977; U.S. Geological Survey, 2011).

significant aquifer drawdown in the SHP, is shallow (< 5 m) (Fig. 16) (McGuire et al., 2003). The rate of groundwater recharge is greatest in the southwestern portion of the SHP, because this area has the thinnest pedogenic calcrete cap rock, low soil clay content, and slightly higher rates of average yearly precipitation (Fig. 15) (Nativ and Gutierrez, 1989; Scanlon et al., 2012). Greater recharge may favor higher rates of uranium transport through the Dockum in this region, increasing the likelihood of deposits forming at areas of discharge in the southern SHP.

4.3. Trapping mechanism

To test if calcrete uranium deposits could form by evaporation of groundwater, Ranalli and Yager (2016) calculated the carnotite saturation index of modern groundwater within the Ogallala aquifer as a function of evaporation. Ranalli and Yager (2016) used water-quality information from 100 groundwater wells downloaded from the USGS National Water Information System database. These wells sampled groundwater throughout the SHP with a distribution like that shown in Figs. 17 and 18 (National Water Information System, 2017). Their calculations indicated that carnotite could precipitate provided that: (1) groundwater composition was initially dominated by a Ca-Mg-SO_4 water type or a Ca-Mg-HCO_3 water type with excess Ca + Mg over that needed to combine with carbonate species; (2) the system was open to CO_2; and (3) evaporation proceeded well beyond the point of carbonate precipitation. Groundwater with the requisite geochemistry to produce carnotite saturation upon evaporation is more common in the southern portion of the SHP based on the spatial distribution of calculated carnotite saturation indices. Saturation indices that predict carnotite would precipitate from modern groundwater are elevated in the southern portion of the SHP in an area that is coincident with elevated vanadium in groundwater and known calcrete uranium occurrences (Fig. 17). Groundwater with elevated uranium concentrations is more widely distributed throughout the region than is elevated vanadium, however the southern portion of the SHP is characterized by more abundant uranium in groundwater (Fig. 18). Ranalli and Yager (2016) initially also modelled the mixing of saline uranium- and vanadium-

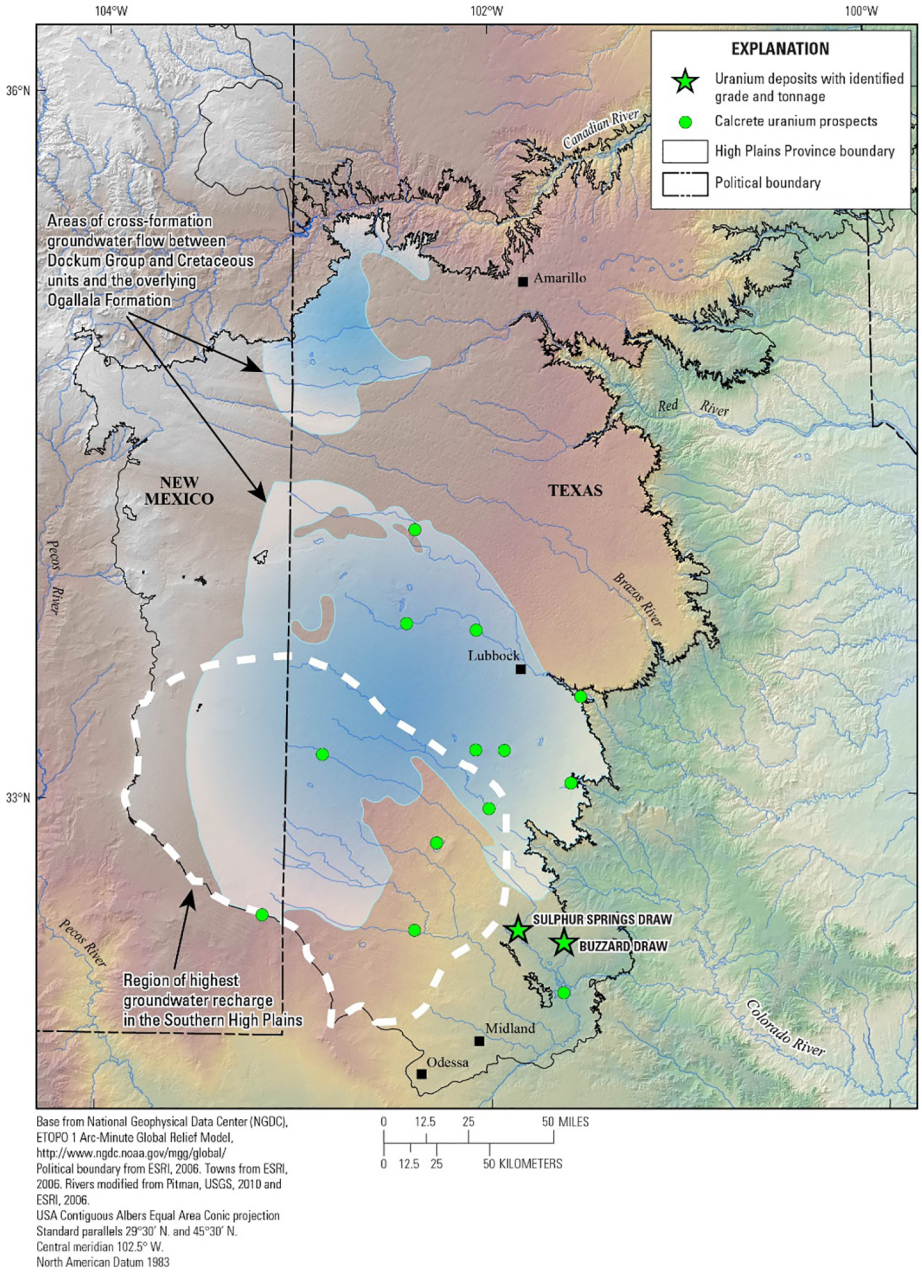


Fig. 15. Areas of highest groundwater recharge, regions where cross-formation groundwater flow is documented among the Dockum Group, Ogallala Formation, and local Cretaceous units as well as the major modern channels (Nativ and Gutierrez, 1989; Scanlon et al., 2012).

enriched groundwater with freshwater, but these conditions did not result in carnotite saturation.

The mineral paragenesis of the Sulfur Springs Draw deposit (Table 3) supports the modelled sequence presented here by the close association of carnotite with carbonate mineral phases. A more precise correlation of the relationship of mineral phases that are predicted by groundwater modelling with those observed in samples collected at Sulfur Springs draw is not expected. This is because the rock exposure is very limited precluding sampling along the entire trace of groundwater as it evolves along the migration path through host rock.

Results from that study illustrate that a single fluid can form calcrete uranium deposits. The mixing of two fluid sources, one for uranium and another for vanadium, as suggested for the Langer-Heinrich and Yeelirrie deposits, is not required. The Ranalli and Yager (2016) study also shows that groundwater in the southern portion of the SHP yields higher calculated carnotite saturation indices and is more likely to form mineral occurrences than areas to the north.

Analysis of host sediments is helpful in identifying the near-surface environments that are favorable for calcrete uranium deposits. Primary dolomite, which is intimately associated with uranium-vanadium mineralization in the SHP, forms infrequently in modern sedimentary environments. One of the rare environments where primary dolomite forms is in saline lakes (Last et al., 2012). Primary dolomite is documented as forming from ponded surface water in modern playa lakes in the SHP, especially near springs and areas of intermittent surface water influx (Parry and Reeves, 1967; Reeves and Parry, 1965). In some calcrete uranium deposits in Australia, and in modern playas in the southwestern United States, uranium is highest where surface and groundwater supply enters playa lakes and associated drainage systems (Leach et al., 1980). The co-occurrence of dolomite and uranium

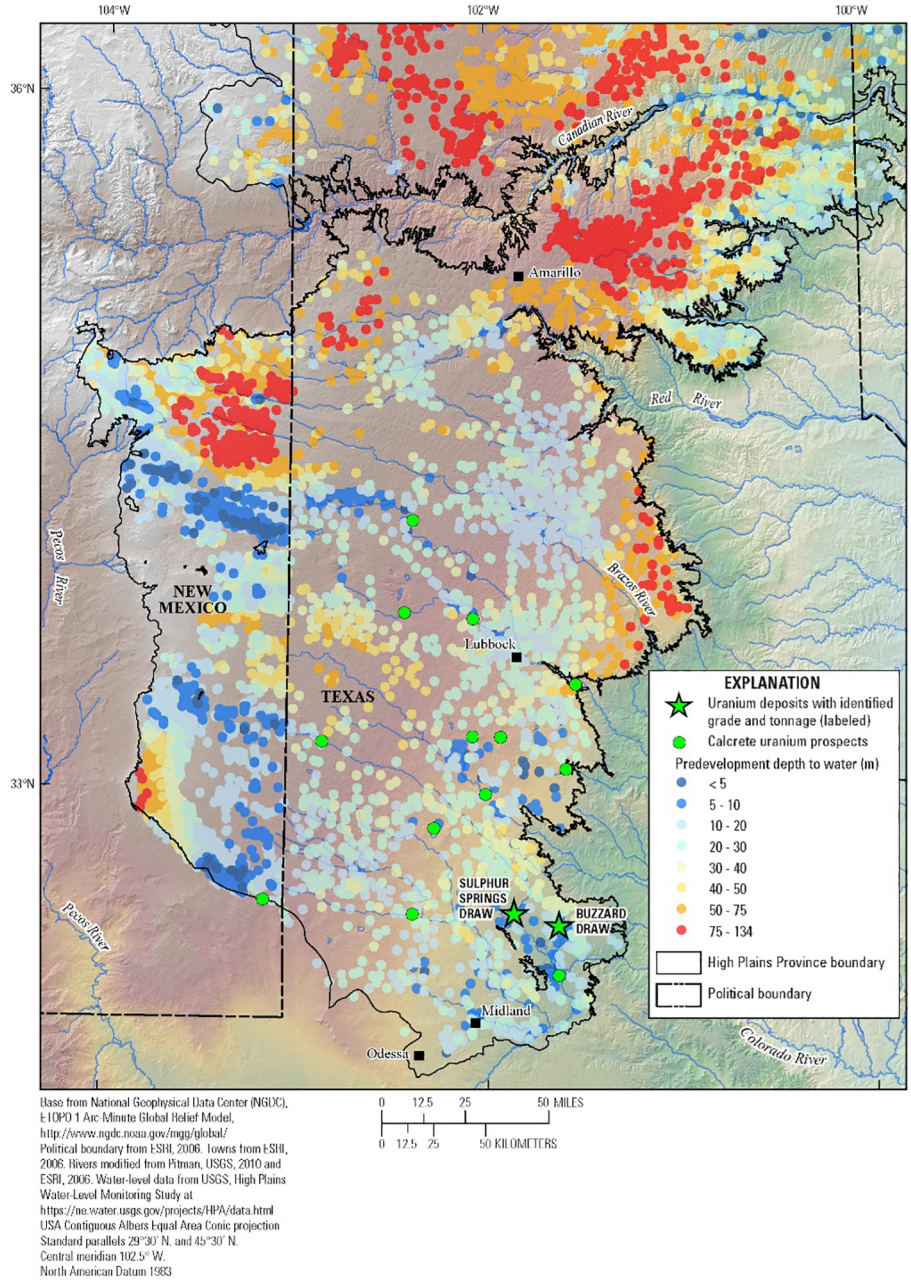


Fig. 16. Pre-development depth to groundwater and uranium occurrences in the SHP. Water depths were measured prior to substantial development of groundwater in the SHP (McGuire et al., 2003).

mineralization in the SHP is evidence that deposits formed in or adjacent to playa lakes where water flow is lateral and slow and surface evaporation is high. Uranium vanadates precipitated from ponded saline surface water and may be associated with areas of water influx both in the past (i.e. 190 ka) as well as more recently. Kerr-McGee searched for these areas by targeting their drilling program to test zones where high and low sulfate groundwater are found in close proximity. The unusually high concentrations of uranium in the dolomite of the Couch Member near Slaton imply extremely high concentrations of dissolved uranium at the time of dolomite precipitation. This condition could be realized near a calcrete uranium deposit undergoing destruction by fresh water. Diversion of U- and V-bearing water to a nearby evaporative setting could then produce U-rich dolomite as an early precipitate.

4.4. Preservation

The Slaton and Lott occurrences crop-out along the eastern SHP escarpment, and were identified partly because they are exposed there. Retreat of the SHP escarpment is estimated at 11 to 18 cm/year (Gustavson et al., 1981). Other uranium occurrences and the two identified calcrete uranium deposits are exposed within modern drainages. Surface denudation is estimated at 0.50 to 2.97 mm/year (Gustavson et al., 1981). Continuing erosion influences the number,

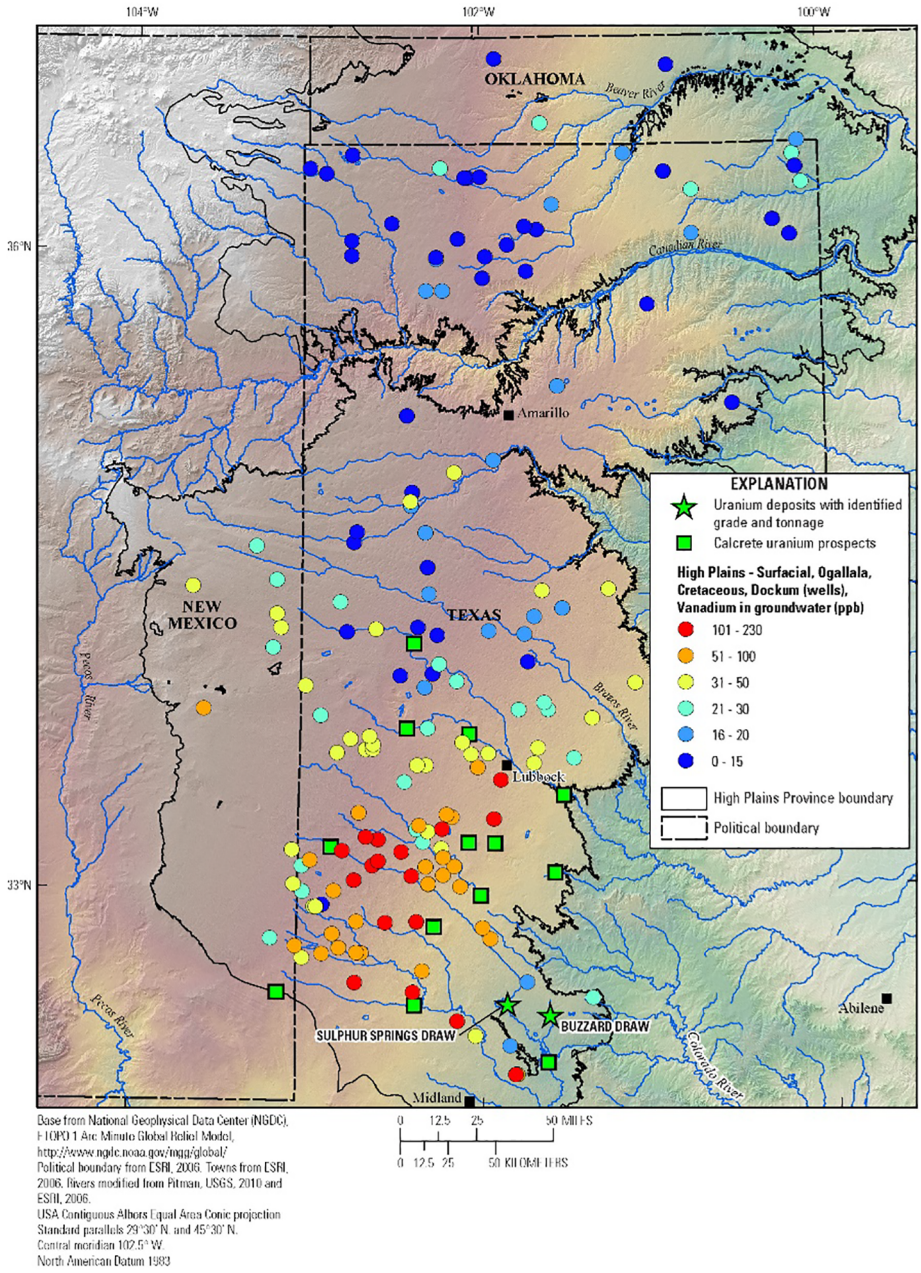


Fig. 17. Vanadium concentration (parts per billion; ppb) in groundwater from wells developed in the Ogallala Formation, Cretaceous units, and Dockum Group, and the location of Kerr-McGee uranium occurrences. Data from National Water Information System (2017).

size, and geometry of preserved calcrete uranium deposits through processes of dissolution, mobilization, and reprecipitation.

5. Summary and conclusions

Calcrete uranium occurrences in the Southern High Plains physiographic province formed near the surface in evaporative environments. Mineralization is hosted in Pliocene to Pleistocene rocks scattered throughout west Texas and easternmost New Mexico. Surface samples collected from one of the larger occurrences, the Sulfur Springs Draw deposit, formed the focus of this study. Here uranyl-vanadates are disseminated in and form coatings on host lacustrine dolomite. U-series disequilibrium dating of the least-mineralized lacustrine-carbonate host rock yield apparent agest of 190 ka. Carnotite and other uranium-vanadate minerals scraped from fracture coatings in the same rock have much younger U-series dates from 8.5 to 3.8 ka. These Holocene ages record the most recent episode(s) of uranium and vanadium mobilization affecting surficial host rocks at the Sulfur Springs Draw deposit. Younger ages of mineralization correspond to an arid interval in the SHP that may have caused higher rates of surface and groundwater evaporation and increased solute supply. Older generations of carnotite mineralization are likely present at depth based on previously reported analyses of core samples by Kerr-McGee, where U-series isotopes that indicated a much closer approach to radioactive equilibrium. Historical fluctuations of the water table at the site of the Sulfur Springs Draw deposit have likely affected the apparent ages through open-system dissolution/reprecipitation of carnotite and other uranyl vanadates.

The source of uranium and vanadium was likely the underlying Upper Triassic Dockum Group, which hosts uranium and vanadium deposits elsewhere in the western United States. This conclusion is supported by the similarity of radiogenic strontium isotopes ($^{87}Sr/^{86}Sr$) measured in Sulfur Springs Draw minerals with those reported for

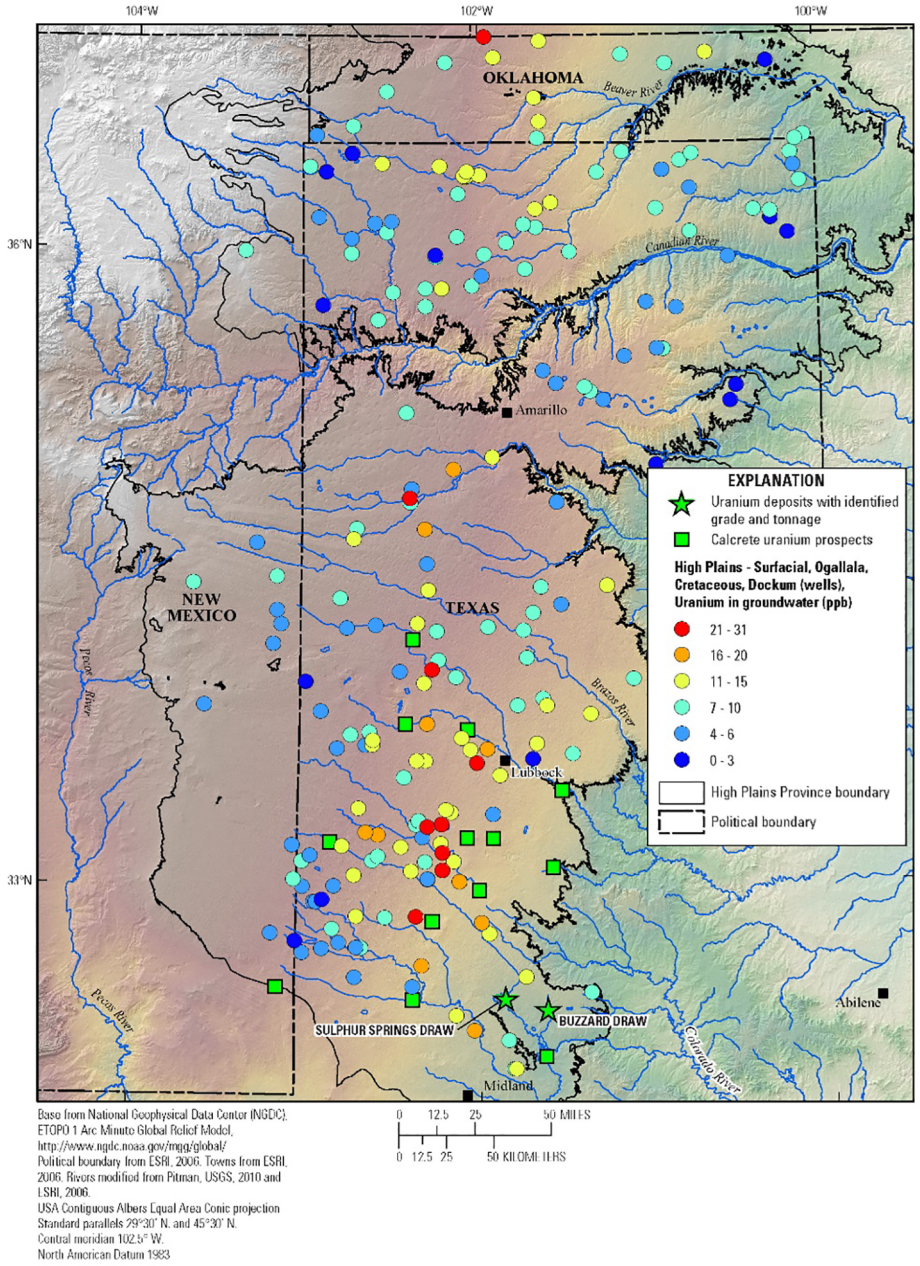


Fig. 18. Uranium concentration (parts per billion; ppb) in groundwater from wells developed in the Ogallala Formation, Cretaceous units, and Dockum Group, and the location of Kerr-McGee uranium occurrences. Data from National Water Information System (2017).

groundwater pumped from Dockum Group aquifers. The two known deposits are found where Pleistocene host rock directly overlies the Dockum, this observation also supports the Dockum as the major source of uranium. Volcanic ash deposits, including the Lava Creek B ash and Guaje Pumice Bed, are interbedded in the Pleistocene host rocks and could also contribute some of the uranium. However, most of the uranium and additional vanadium were likely sourced in underlying geologic units and introduced by upward transport of groundwater that continues to be documented in portions of the study area.

Modelling of modern groundwater indicates that carnotite could precipitate during evaporation of some U- and V-bearing groundwater of appropriate major-ion composition (Ranalli and Yager, 2016). Favorable compositional characteristics include high concentrations of dissolved sulfate and Ca and Mg concentrations more than that needed to combine with dissolved carbonate species. Instances of favorable major-ion composition combined with generally higher concentrations of dissolved vanadium in the southern portion of the SHP suggest that this area is more likely to produce waters saturated in carnotite and calcrete uranium deposits. Occurrences in the southern portion of the SHP are in or near modern drainage systems that trend northwest to southeast. These drainages have persisted throughout the Pleistocene and Holocene. The two identified calcrete uranium deposits are found near ephemeral lakes. Ephemeral lakes represent sluggish portions of the drainages where uranium- and vanadium-bearing surface water and groundwater would be continually supplied and subjected to evaporative concentration under ambient semiarid to arid conditions. Alternating wet and dry periods in the SHP from the Pliocene through Holocene pumped groundwater and surface water through surface lacustrine and fluvial systems, resulting in multiple mineralizing pulses. Preservation of calcrete uranium deposits in the SHP is threatened by ongoing erosion along the eastern escarpment and within existing drainages.

Acknowledgments

This work was funded by the US Geological Survey and is part of a project to assess the potential (undiscovered) uranium resources of the United States. Without help from Uranium Energy Corporation, and in particular Clyde Yancey and Rick Edge, who facilitated access to historical Kerr-McGee corporation files, this work could not have been completed. Elmira Wan at the USGS tephrochronology laboratory analyzed and interpreted a source for volcanic ash collected near the Sulfur Springs Draw deposit outcrop (Table 1). Mark Mihalasky (U.S. Geological Survey, USGS) and the International Atomic Energy Agency provided locations for the grade and tonnage of world calcrete uranium occurrences used in Fig. 1. Mihalasky created Fig. 2 using International Atomic Energy Agency data. John Wallis (Serrano IT Services) expertly drafted multiple versions of the figures used in this paper. Thanks to Virginia McGuire (USGS) for providing predevelopment groundwater level data for the Southern High Plains used in Fig. 16. Any use of trade, firm, or product names is for descriptive purposes only and does not imply endorsement by the U.S. Government. We would like to acknowledge the foresight of co-author George Breit who initiated the search for calcrete uranium in the United States, arguing that these types of deposits should exist based on his application of world deposit models. He was right.

Appendix A. Analytical techniques

SEM/EDAX

A scanning electron microscope (SEM) equipped with an energy-dispersive X-ray spectroscopy system (EDS) was used to examine uranium mineralization in samples from the deposit. Secondary and backscattered electron images of the samples were acquired with a FEI Quanta 450 Field Emission Gun SEM operating at 15 and 20 kV, using an approximately 2-nanoampere beam current. Energy-dispersive spectra were collected for 30 s live-count time with an EDAX Apollo X silicon drift detector.

Fission track analysis

A polished thin section and overlying "detector" of low-U muscovite mica were neutron-irradiated in a research reactor to induce fission of ^{235}U in the thin section material. During irradiation (2.5×10^{12} neutrons/cm^2-sec. for 4 h), fission fragments recoil from the surface of the thin section and pass into the overlying sheet of mica. The passage of fission fragments causes linear paths of damage (tracks) in the mica that are made more visible by subsequent etching of the recovered mica in 48% hydrofluoric acid. Areas of high fission track density in the mica correspond to areas of high U concentration in the thin section, as related by comparative observations with an optical microscope. Fission tracks appear dark under transmitted light, but the thin section-scale image of the mica detector was produced by an optical scan against a black background to increase contrast. In this "negative" image the areas of highest fission track density appear lightest in color.

Radiogenic strontium and uranium isotopes

Data given in Table 4 were determined at U.S. Geological Survey (USGS) laboratories in Denver, Colorado. Samples included a non-mineralized, U-rich, pink, finely laminated dolomite (Ziel-3B-USGS) collected from the Couch Member of the Ogallala Formation near Slaton, Texas. Subsamples were obtained by drilling shallow 1-mm-diameter holes in different parts of the polished surface and collecting the resulting powder (Fig. A-1), and uranium isotope series results are shown in Fig. A-2. Samples from the Sulfur Springs Draw ore zone consisted of massive white, porcelain-like, lacustrine dolomite and included subsamples with U-poor matrix and very minor carnotite present on fracture surfaces (non-mineralized host; SSD15-01A), and subsamples with U-rich matrix and very noticeable carnotite on multiple surfaces (mineralized host; SSD15-01C). Multiple aliquots were collected by excavating small trenches in matrix material using a 1-mm-diameter carbide dental bur or scraping carnotite-rich fracture surfaces (Fig. A-3). Samples from the Sulfur Springs Draw area outside of the ore zone consisted of five thin section billets with a wide range of textures (SSD15-02 to SD15-06; Fig. A-4). Uranium minerals were not identified on any of those samples. Subsamples were collected by excavating small trenches on slabbed surfaces as above.



Fig. A-1. Photograph of specimen Ziel-3B-USGS (24 × 46 mm) collected from the Slaton Quarry near Slaton, Texas showing subsamples collected by drilling shallow holes.

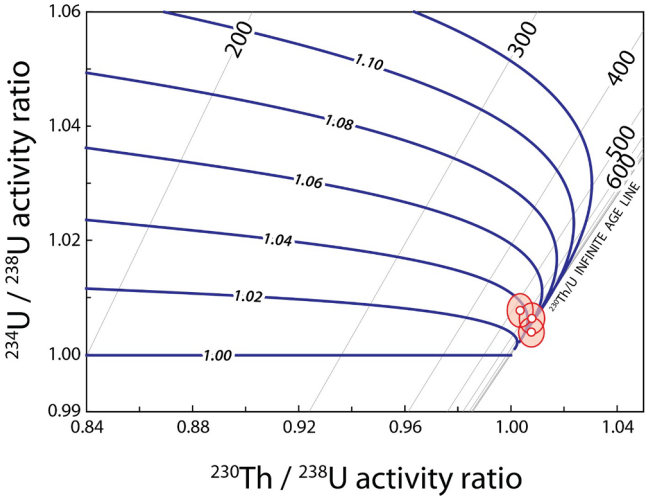


Fig. A-2. Uranium-series evolution plot of $^{234}U/^{238}U$ and $^{230}Th/^{238}U$ activity ratios for analyses of sample Ziel-3B-USGS (Fig. A-1, Table 3). Dark curved lines are the loci of compositions derived from closed-system decay of ^{234}U and in-growth of ^{230}Th from $^{234}U/^{238}U$ activity ratios of 1.00 to 1.20. Straight, light lines are isochrons labeled in thousands of years before present. Data points (in red) are shown along with 95%-confidence error ellipses. (For interpretation of the references to color in this figure legend, the reader is referred to the web version of this article.)

Powdered subsamples were weighed in 7-ml Teflon® PFA vials, then wetted with deionized water. Small amounts of a highly purified mixed U-Th tracer solution with known quantities of ^{236}U, ^{233}U, and ^{229}Th were added, followed by addition of high-purity concentrated nitric acid to digest the carbonate fraction. Vials were capped, heated overnight on a 120 °C hotplate, and then taken to dryness under ULPA-filtered airflow. Digested salts were dissolved in 7 N nitric acid. Any remaining residue was separated and digested in the same vials using concentrated hydrofluoric and nitric acids. After drying, the resulting salts were dissolved in 7 N nitric acid and added to the original digestion. Therefore, all analyses were made on total digestions of the samples to eliminate any laboratory fractionation of U and Th. Sr analyses were made on the same total digestions.

Standard ion chromatographic separations with Biorad™ AG1 × 8 (0.5 ml of 200-400 mesh) resin were used to purify uranium and thorium. Strontium separates were made on the same solutions by piggybacking separate columns containing 0.25 ml of Sr-Spec™ resin beneath U columns. After initial washes of the loaded columns using 7 N nitric acid, U and Sr columns were separated and processed independently to obtain purified U–Th, and Sr cuts.

Resulting U salts were loaded on Re filaments placed on evaporation side of double-filament assemblies. Thorium salts were loaded along with a graphite suspension on single Re-filament assemblies. Isotope ratios were obtained using a Thermo Finnigan Triton™ thermal ionization mass spectrometer equipped with an RPQ electrostatic filter which reduced abundance sensitivity on a theoretical ^{237}U mass to < 5 ppb. Ratios were determined using a single MasCom™ electron multiplier operating in peak-jumping mode. Sr salts were loaded on single Re center filaments along with a small amount of tantalum-oxide. $^{87}Sr/^{86}Sr$ ratios were collected on the same instrument using faraday cups and a triple-jump multi-dynamic peak-hopping routine.

Raw U and Th data were corrected for mass fractionation, spike contributions, and procedural blanks, and were normalized relative to a standard value for NIST SRM 4321B of $^{234}U/^{238}U$ atomic ratio of 0.0000529. Total-process blank contributions varied between 5 and 10 picograms of uranium and 10–50 picograms of thorium. $^{87}Sr/^{86}Sr$ ratios were normalized for instrumental fractionation using the accepted value for $^{86}Sr/^{88}Sr$ value of 0.1194. Data for $^{84}Sr/^{86}Sr$ were also collected during the same run to monitor the effectiveness of the fractionation correction. Total-process blank contributions for Sr varied between 30 and 100 picograms.

Uranium isotopic compositions of the international U-isotope standard, NIST SRM4321B, determined over the same period of data collection yielded results within analytical uncertainties of the certified $^{234}U/^{238}U$ value of 0.0000529 ± 0.0000011. Results for a USGS in-house secular equilibrium standard derived from a 69 million-year-old uranium ore from the Schwartzwalder mine (Ludwig et al., 1985) yielded results that are analytically indistinguishable from the secular equilibrium value of 1.0000 ($^{234}U/^{238}U$ AR = 0.9997 ± 0.0032 [± 2 × standard deviation, N = 65], and $^{230}Th/^{238}U$ AR = 0.9999 ± 0.0051 [± 2 × standard deviation, N = 59]). Analyses of a USGS late Pleistocene *Acropora* coral dating standard (mean age of 119.6 ± 1.9 ka for N = 17, (Watanabe and Nakai, 2006)) processed in an identical manner as the unknown samples yielded an average age of 119.8 ± 1.7 ka and an initial $^{234}U/^{238}U$ activity ratio of 1.153 ± 0.006 (± 2 × standard deviation, N = 42). All uncertainties presented herein are given at the 95% confidence level (± 2σ).

The mean $^{87}Sr/^{86}Sr$ value obtained for 304 analyses of the international Sr-isotope standard, NIST SRM987, was 0.710250 ± 0.000008 (2 × standard deviation), which is within uncertainty of the accepted value of 0.710248 ± 0.000006 (McArthur et al., 2001). The $^{87}Sr/^{86}Sr$ values determined for unknown samples are normalized to the accepted value using the average value obtained for each batch of analyses. A secondary USGS Sr-isotope standard, EN-1, analyzed as an unknown with each batch, yielded a mean normalized $^{87}Sr/^{86}Sr$ value of 0.709174 ± 0.000014 (2 × standard deviation for 206 analyses) which is identical to the accepted value of 0.709174 ± 0.000002 (± 2 × standard error; (McArthur et al., 2006).

U-series ratios include measurements of $[^{232}Th/^{238}U]$, $[^{230}Th/^{238}U]$, and $[^{234}U/^{238}U]$ (square brackets indicate values are given as activity ratios converted from atomic ratios using accepted values for radioactive decay constants). Measureable amounts of common thorium (that is, ^{232}Th) imply that some ^{230}Th not associated with the in-situ decay of parent isotope ^{234}U is present in the sample. To avoid calculating erroneously old $^{230}Th/U$ ages, any initial ^{230}Th derived from detrital sources must be eliminated. This is done mathematically based on the measured $[^{232}Th/^{238}U]$, and an assumption about the isotopic composition of the thorium-bearing detrital component (Ludwig and Paces, 2002). The detrital component is assumed to have an atomic Th/U of 4 with the following activity ratios and 2σ errors: $[^{232}Th/^{238}U] = 1.276 \pm 0.64$; $[^{234}U/^{238}U] = 1.0 \pm 0.1$; and $[^{230}Th/^{238}U] = 1.0 \pm 0.25$. Detrital corrected ratios are used to calculate $^{230}Th/U$ ages, initial $[^{234}U/^{238}U]$ and associated errors using conventional U-series age equations (Ludwig, 2012).

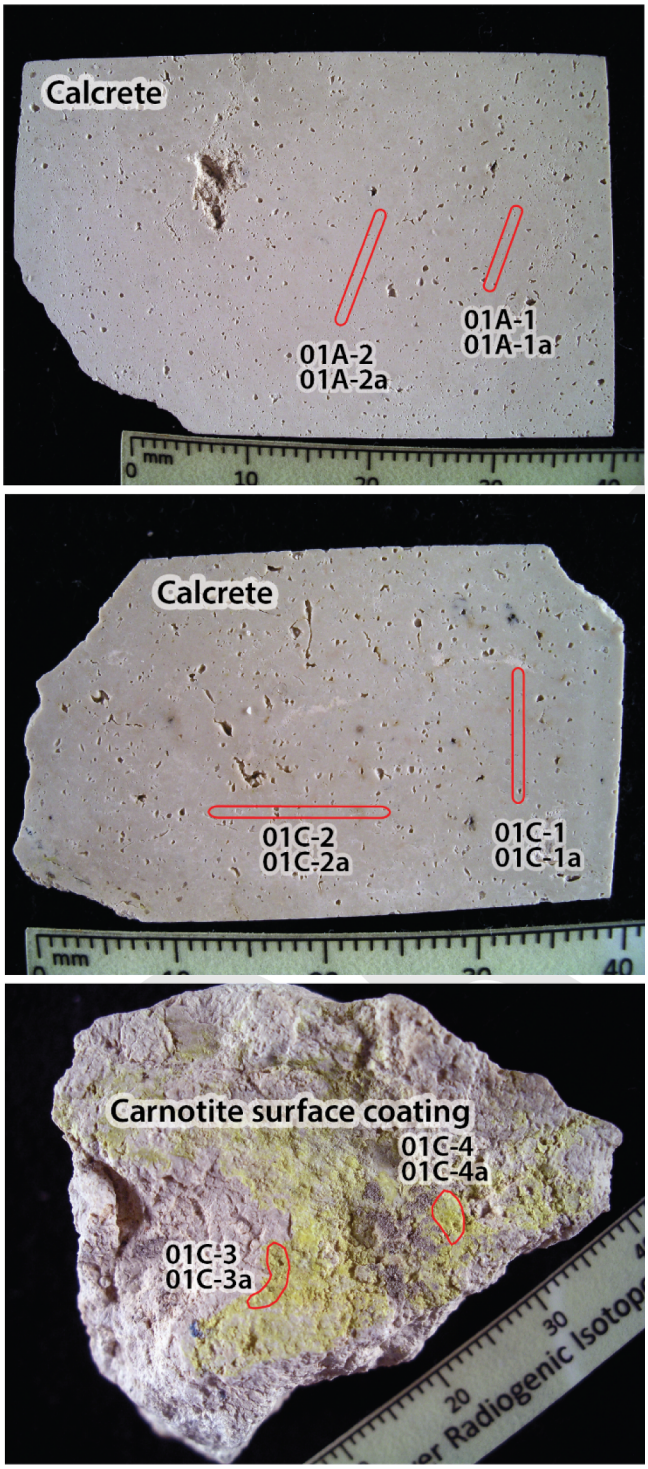


Fig. A-3. Photograph of sample SSD15 collected from the Sulfur Springs Draw ore zone showing subsampling locations. Sample 01A (top) is from non-mineralized host rock, sample 01C-1 and 01C-2 (middle) is from the matrix of mineralized host rock and sample 01C-4, 01C-4 (bottom) is scrapings of ore from a mineralized surface. Scale bar shows mm and cm increments. For sample location and description see Van Gosen and Hall, 2017.

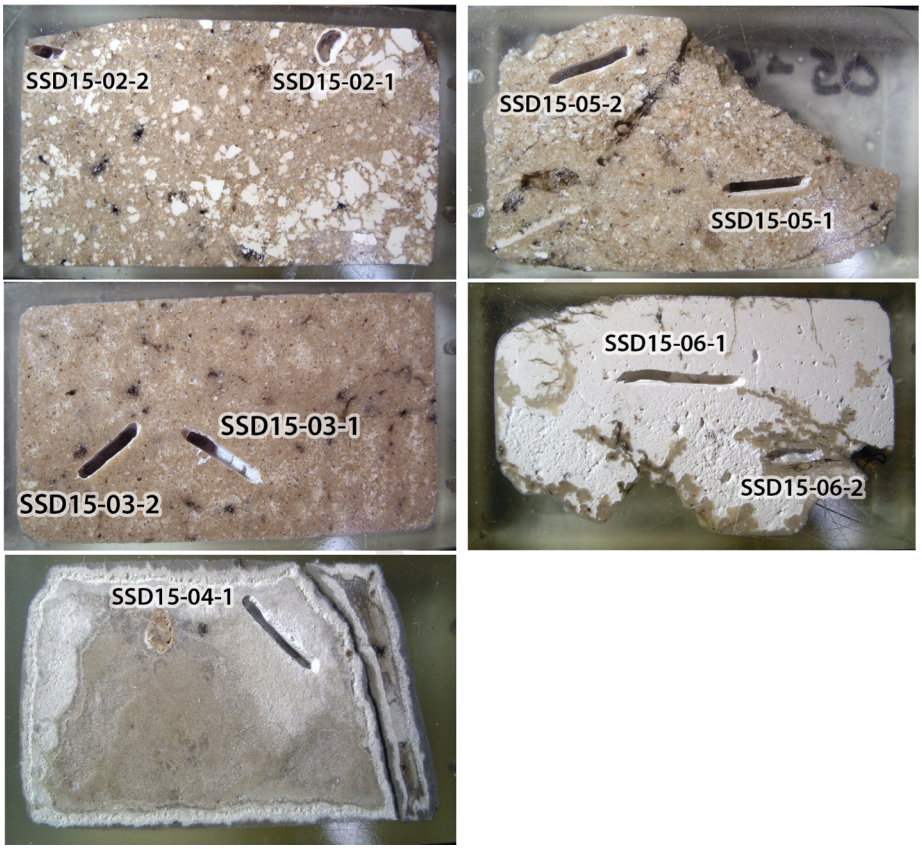


Fig. A-4. Subsampled portions of 24 × 46 mm thin section billets from samples collected outside the ore zone. For sample location and description see Van Gosen and Hall (2017).

Appendix B. Supplementary data

Supplementary data to this article can be found online at https://doi.org/10.1016/j.oregeorev.2019.03.036.

References

Amaral, E.J., 1979. National uranium resource evaluation, Plainview quadrangle, Texas. US Department of Energy Open File Report GJQ-001(79). 7 p. plus plates and tables. 1:24,000.
Barczak, V.J., 1974. Examination of rocks from Southern High Plains Region. Internal Kerr-McGee Corporation correspondence, Jan. 11, 3 p.
Barczak, V.J., 1977. Occurrence of Carnotite in Sulfur Springs Draw Depsoit. Internal Kerr-McGee Corporation correspondence, January 9, 1977. 25 p.
Bianconi, F., Borshoff, J., 1984. Surficial uranium occurrences in the United Republic of Tanzania. In: Toens, P.D. (Ed.), Surficial Uranium Deposits. International Atomic Energy Agency IAEA-TECHDOC-322. International Atomic Energy Agency, Vienna, pp. 231–235.
Boyle, D.R., 1974. The genesis of surficial uranium deposits. In: Toens, P.D. (Ed.), 1984. Surficial Uranium Deposits. International Atomic Energy Agency IAEA-TECHDOC-322. International Atomic Energy Agency, Vienna, pp. 45–52.
Bradley, R.G., Kalaswad S., 2003. The Groundwater Resources of the Dockum Aquifer in Texas. Texas Water Development Board Report 359. 73 p.
Butt, C.R.M., Horwitz, R.C., Mann, A.W., 1977. Uranium occurrences in calcrete and associated sediments in Western Australia. CSIRO Research Laboratories Division of Mineralogy Report F.P. 16. 67 p.
Butt, C.R.M., Graham, J., 1981. Sodian potassian hydroxonian meta-autunite: first natural occurrence of an intermediate member of a predicted solid solution series. Am. Mineral. 66, 1068–1072.
Cameron, E., 1984. The Yeelirrie calcrete uranium deposit, Western Australa. In: Toens, P.D. (Ed.), Surficial Uranium Deposits. International Atomic Energy Agency, Vienna, pp. 157–164.
Campbell, J.A., Steele, B.A., 1976. Uranium potential of Permian rocks in the southwestern United States. U.S. Geological Survey Open-File Report 76–529, 26 p.
Carlisle, D., 1978. The Distribution of Calcretes and Gypcretes in Southwestern United States and their Uranium Favorability Based on a Study of Deposits in Western Australia and South West Africa (Namibia). U.S. Department of Energy Open File Report GJBX-29(78), pp. 274.
Carlisle, D., 1983. Concentration of uranium and vanadium in calcretes and gypcretes. Geol. Soc. London Special Public. 11, 185–195.
Carlisle, D., 1984. Surficial uranium occurrences in relation to climate and physical setting. In: Toens, P.D. (Ed.), Surficial Uranium Deposits. International Atomic Energy Agency, Vienna, pp. 25–35.
Chen, X.Y., Lintern, M.J., Roach, I.C., 2002. Calcrete: characteristics, distribution and use in mineral exploration. CRC LEME Perth 166, pp.
Cheng, H., Edwards, R.L., Shen, C.-C., Polyak, V.J., Asmerom, Y., Woodhead, J., Hellstrom, J., Wang, Y., Kong, X., Spötl, C., Wang, X., Alexander Jr., E.C., 2013. Improvements in ^{230}Th dating, ^{230}Th and ^{234}U half-life values, and U-Th isotopic measurements by multi-collector inductively coupled plasma mass spectrometry. Earth Planet. Sci. Lett. 371–372, 82–91.
Crabb, D., Dudley, R., Mann, A.W., 1984. Hinkler well - centipede uranium deposits. In: Toens, P.D. (Ed.), Surficial Uranium Deposits. International Atomic Energy Agency, Vienna, pp. 133–136.
Dahlkamp, F.J., 2010. Uranium Deposits of the World – Part I. Springer, Berlin, Heidelberg, pp. 26.
Eifler, G.K.J., 1967. Geologic Atlas of Texas, Lubbock Sheet, scale 1:200,000. Bureau of Economic Geology. University of Texas at Austin, Austin Texas 1 plate.
Eifler, G.K.J., Frye, J.C., Leonard, A.B., 1974. Geologic Atlas of Texas, Big Spring Sheet, scale 1:250,000. Bureau of Eocnomic Geology. University of Texas at Austin, Austin, Texas, pp. 6 plus 1 plate.

Fallin, J.A.T., 1989. Hydrogeology of Lower Cretaceous strata under the Southern High Plains of Texas and New Mexico. Texas Water Development Board Report No. 314, 39 p.
Fallis, J.F.J., 1973. Drilling Recommendation Slaton Area, Crosby, Lubbock and Lynn Counties, Texas. Internal Kerr-McGee Corporation correspondence, pp. 5.
Finch, W.I., 1972. Uranium in eastern New Mexico. U.S. Geological Survey Open-File Report 72-117. 19 p.
Finch, W.I., 1975. Uranium in West Texas - Paper delivered June 3, 1975, AAPG-SEPM Rocky Mountain Section Meeting, Albuquerque, New Mexico. U.S. Geological Survey Open-File Report 75-356. 20 p.
Fletcher, K.E.K., Sharp, W.D., Kendrick, K.J., Behr, W.M., Hudnut, K.W., Hanks, T.C., 2010. ^{230}Th/U dating of a late Pleistocene alluvial fan along the southern San Andreas Fault. Geol. Soc. Am. Bull. 122, 1347–1359.
Frye, J.C., Leonard, A.B., 1957. Studies of Cenozoic geology along eastern margin of Texas high plains, Armstrong to Howard Counties. University of Texas Bureau of Economic Geology Report of Investigations, pp. 38.
U.S. Geological Survey, 2011. [database] Mineral Resource Data System. < https://mrdata.usgs.gov/mrds/ > .
Gurdak, J.J., Roe, C.D., 2010. Rechange rates and chemistry beneath playas of the high plains aquifer - a literature review and synthesis. U.S. Geol. Survey Circular 1333, 46 p.
Gustavson, T.C., Finley, R.J., Baumgardner, R.W., 1981. Retreat of the caprock escarpment and denudation of the rolling plains in the Texas panhandle. Environ. Eng. Geosci. xviii, 413–422.
Gutentag, E.D., Heimes, F.J., Krothe, N.C., Luckey, R.R., Weeks, J.B., 1984, Geohydrology of the High Plains aquifer in parts of Colorado, Kansas, Nebraska, New Mexico, Oklahoma, South Dakota, Texas and Wyoming. U.S. Geological Survey Professional Paper 1400-B. 63 p.
Hall, S.M., Mihalasky, M.J., 2017. [dataset] Grade, tonnage and location data for world calcrete-type surficial uranium deposits. U.S.G.S. Data release DOI:10.5066/F7MS3RQS.
Hall, S.M., Mihalasky, M.J., Van Gosen, B.S., 2017. Assessment of undiscovered resources in calcrete uranium deposits, Southern High Plains region of Texas, New Mexico and Oklahoma, 2017. U.S. Geological Survey Fact Sheet 2017-3078. 2 p.
Hartleb, J.W.O., 1988. The Langer Heinrich uranium deposit: Southwest Africa/Namibia. Ore Geol. Rev. 3, 277–287.
Hill, A.G., Kucks, R.P., Ravat, D., 2009. Aeromagnetic and aeroradiometric data for the conterminous United States and Alaska from the National Uranium Resource Evaluation (NURE) Program of the U.S. Department of Energy. U.S. Geological Survey Open-File Report 2009-1129. < https://pubserusgsgov/publication/ofr20091129 > .
Holliday, V.T., 1985. Holocene soil – geomorphological relations in a semi-arid environment: the Southern High Plains of Texas. In: Boardman, J. (Ed.), Soils and Quaternary Landscape Evolution. John Wiley, New York, pp. 325–357.
Holliday, V.T., 1989. The Blackwater Draw Formation (Quaternary): a 1.4-plus-m.y. record of eolian sedimentation and soil formation on the Southern High Plains. Geol. Soc. Am. Bull. 101, 1598–1607.
Holmberg, H.W., Kirsh, E.J., 1977. Regional evaluation and drilling recommendation, Southern High Plains. Internal Kerr-McGee corporation correspondence, December 6, 1977. 10 p.
International Atomic Energy Agency, 2009. World distribution of uranium deposits (UDEPO) with uranium deposit classification. IAEA-Tecdoc-1629. 117 p.
Izett, G.A., 1981. Volcanic ash beds: recorders of upper Cenozoic silicic pyroclastic volcanism in the western United States. J. Geophys. Res. 86 (B11), 10200–10222.
Jaireth, S., Roach, I.C., Bastrakov, E., Liu, S., 2015. Basin-related uranium mineral systems in Australia; a review of critical features. Ore Geol. Rev. 76, 360–394.
Kinnaird, J.A., Nex, P.A., 2016. Uranium in Africa. Episodes 39, 335–359.
Knowles, T., Nordstrom, P., Klemt, W.B., 1984. Evaluating the Ground-water Resources of the High Plains of Texas. Texas Department of Water Resources Report 288, pp. 113.
Krish, E.J., 1977a. Ore Reserve Calculations, Sulfur Springs Draw, Texas. Internal Kerr-McGee Corporation correspondence, pp. 2.
Krish, E.J., 1977b. Regional Evaluation of the Southern High Plains - Interim Report. Internal Kerr-McGee Corporation correspondence, pp. 8.
Last, F.M., Last, W.M., Halden, N.M., 2012. Modern and late Holocene dolomite formation: Manito Lake, Saskatchewan, Canada. Sedimentary Geol. 281, 222–237.
Leach, D.L., Puchlik, K.P., Glanzman, R.K., 1980. Geochemical exploration for uranium in playas. J. Geochem. Exploration 13, 251–283.
Lucas, S.G., Anderson, O.J., 1995. Dockum (upper Triassic) stratigraphy and nomenclature. West Texas Geol. Survey Bull. 34–7, 5–11.
Ludwig, K.R., 2012. User's Manual for Isoplot 3.75, A Geochronological Toolkit for Microsoft Excel. Berkeley Geochronological Center Special Publication No 5, Berkeley, CA, pp. 75.
Ludwig, K.R., Paces, J.B., 2002. Uranium-series dating of pedogenic silica and carbonate, Crater Flat, Nevada. Geochim. Cosmochim. Acta 66, 487–506.
Ludwig, K.R., Wallace, A.R., Simmons, K.R., 1985. The Schwartzwalder uranium deposit, II: age of uranium mineralization and Pb-isotope constraints on genesis. Econ. Geol. 80, 1858–1871.
Mann, A.W., Deutscher, R.L., 1978. Genesis principles for the precipitation of Carnotite in calcrete drainages in Western Australia. Econ. Geol. 73, 1724–1737.
Mann, A.W., Horwitz, R.C., 1979. Groundwater calcrete deposits in Australia some observatiosn from Western Australa. J. Geol. Soc. Australia 26, 293–303. https://doi.org/10.1080/00167617908729092.
Matthews, N.E., Vasquez, J.A., Calvert, A.T., 2015. Age of the Lava Creek supereruption and magma chamber assembly at Yellowstone based on ^{40}Ar/^{39}Ar and U-Pb dating of sanidine and zircon crystals. Geochem., Geophys., Geosyst. 16, 2508–2528.
McArthur, J.M., Howarth, R.J., Bailey, R.R., 2001. Strontium isotope stratigraphy: LOWESS version 3: best fit to the marine Sr-isotope curve for 0–509 Ma and accompanying look-up table for deriving numerical age. J. Geol. 109, 155–170.
McArthur, J.M., Rio, D., Massari, F., Castradori, D., Bailey, T.R., Thirlwall, M., Houghton, S., 2006. A revised Pleocene record for marine-^{87}Sr/^{86}Sr used to date an interglacial event recorded in the Cockburn Island Formation, Antarctic Peninsula. Palaeogeogr., Palaeoclimatol., Palaeoecol. 242, 126–136.
McGowen, J.H., Granata, G.E., Seni, S.J., 1977. Depositional Systems, Uranium Occurrence and Postulated Ground-water History of the Triassic Dockum Group. Texas panhandle-eastern New Mexico. Texas Bureau of Economic Geology, The University of Texas at Austin, pp. 104.
McGowen, J.H., Seni, S.J., Andersen, R.L., Thurwachter, J.E., 1981. In: National Uranium Resource Evaluation Lubbock Quadrangle Texas GJQ-012 (81). U.S. Department of Energy, Grand Junction, CO, pp. 48 48 plates.
McGuire, V.L., Johnson, M.R., Schieffer, R.L., Stanton, J.S., Sebree, S.K., Verstraeten, I.M., 2003. Water storage and approaches to ground-water management, high plains aquifer. U.S. Geol. Survey Circular 1243, 51 p.
National Water Information System, 2017. [database]. U.S. Geological Survey. < https://waterdata.usgs.gov/nwis > .
Nativ, R., Gutierrez, G.N., 1989. Hydrogeology and hydrochemistry of Cretaceous aquifers, Southern High Plains, U.S.A. J. Hydrol. 108, 79–109.
Nativ, R., Smith, D.A., 1987. Hydrogeology and geochemistry of the Ogallala aquifer, Southern High Plains. J. Hydrol. 91, 217–253.
Neuendorf, K.K.E., Mehl, J.P., Jackson, J.A., 2011. Glossary of Geology, fifth ed. American Geosciences Institute, Alexandria, Virginia, pp. 783.
Paces, J.B., 2014. ^{230}Th/U age supporting Hanford site-wide probabilistic seismic hazard analysis. In: U.S. Geological Survey Administrative Report to the Department of Energy Pacific Northwest National Laboratory, pp. 28. https://doi.org/10.2172/1128696.
Paces, J.B., 2015. ^{230}Th/U ages Supporting Geologic Map of the Masters 7.5' Quadrangle, Weld and Morgan Counties, Colorado. 1:24,000 In: Berry, M.E., Slate, J.L., Paces, J.B., Hanson, P.R., Brandt, T.R. (Eds.), Geologic Map of the Masters 7.5' Quadrangle, Weld and Morgan Counties, Colorado. U.S .Geological Survey Scientific Investigations Map. https://doi.org/10.3133/sim3344.
Paces, J.B., Whelan, J.F., 2012. The paleohydrology of unsaturated and saturated zones at Yucca Mountain, Nevada, and vicinity. In: Stuckless, J.S. (Ed.), Hydrology and Geochemistry of Yucca Mountain and Vicinity, Southern Nevada and California, pp. 219–276.
Pagel, M., 1984. Petrology, mineralogy and geochemistry of surficial uranium deposits. In: Toens, P.D. (Ed.), Surficial Uranium Deposits. International Atomic Energy Agency, Vienna, pp. 37–44.
Parry, W.T., Reeves Jr., C.C., 1967. Preliminary report; Primary soft sediment dolomite from pluvial Lake Mound, Lynn and Terry counties, Texas. Texas J. Sci. 19, 132–137.
Paskevich, V., 2006. State_bounds: internal United States boundaries. U.S. Geological Survey Open-File Report 2006-1046.
Pierce, A.P., Gott, G.B., Mytton, J.W., 1964. Uranium and helium in the Panhandle gas field Texas, and adjacent areas. U.S. Geological Survey Professional Paper 454-G. 57 p.
Qi, S., 2010. Digital Map of Aquifer Boundary for the High Plains Aquifer in Parts of Colorado, Kansas, Nebraska, New Mexico, Oklahoma, South Dakota, Texas, and Wyoming. U.S. Geological Survey Data Series, pp. 543.
Ranalli, A.J., Yager, D.B., 2016. Use of mineral/solution equilibrium calculations to assess the potential for carnotite precipitation from groundwater in the Texas Panhandle, USA. Appl. Geochem. 73, 118–131.
Reedy, R.C., Scanlon, B.R., Bruce, B., McMahon, P.B., Dennehy, K.F., Ellett, K., 2003. Groundwater Recharge in the Soutern High Plains. Appendix A to the Groundwater Availability Model (GAM), Southern portion of the Ogallala Aquifer. Texas Water Development Board, Austin, TX, pp. 15.
Reedy, R.C., Scanlon, B.R., Walden, S., Strassberg, G., 2011. Naturally Occurring Groundwater Contamination in Texas. Texas Water Development Board, Austin, TX, pp. 203.
Reeves Jr., C.C., 1966. Pluvial lake basins of West Texas. J. Geol. 74, 269–291.
Reeves Jr., C.C., 1970. Origin, classification and geologic history of caliche on the Southern High Plains, Texas and eastern New Mexico. J. Geol. 78–3, 352–363.
Reeves Jr., C.C., 1990. A proposed sequential development of lake basins, Southern High Plains, Texas and New Mexico. In: Gustavson, T.C. (Ed.), Geologic Framework and Regional Hydrology; Upper Cenozoic United States, Conference Proceedings. pp. 209–232.
Reeves Jr., C.C., Parry, W.T., 1965. Geology of West Texas pluvial lake carbonates. Am. J. Sci. 263, 606–615.
Rich, J., 2013. A 250,000-year record of lunette dune accumulation on the Southern High Plains, USA and implications for past climates. Quaternary Sci. Rev. 62, 1–20.
Rogers, J.J.W., Adams, J.A.S., 1978. Uranium 92-E Abundances in Common Igneous Rocks. In: Wedopohl, K.H. (Ed.), Handbook of Geochemistry Vol II/5. Springer-Verlag, Berlin, pp. 442.
Scanlon, B.R., Nicot, J.P., Reedy, R.C., Kurtzman, D., Mukherjee, A., Nordstrom, D.K., 2009. Elevated naturally occuring arsenic in a semiarid oxidizing system, Southern High Plains aquifer, Texas, USA. Appl. Geochem. 24, 2061–2071.
Scanlon, B.R., Faunt, C.C., Longuevergne, L., Reedy, R.C., Alley, W.M., McGuire, V.L., McMahon, P.B., 2012. Groundwater depletion and sustainability of irrigation in the U.S. High Plains and Central Valley. Proc. Natl. Acad. Sci. U.S.A. 109, 9320–9325.
Schurman, S., 1981. Quarterly Summary Sheet - Seminole Prospect. Internal company correspondence, Energy Reserves Group, pp. 5.
Seni, S.J., McGowen, J.H., Risner, R.S., 1980. National uranium resource evaluation, Amarillo qaudrangle, Texas. U.S. Department of Energy Open File Report GJQ-013(81). 24 p, 26 plates.
Sharp, W.D., Ludwig, K.R., Chadwick, O.A., Amundson, R., Glaser, L.L., 2003. Dating fluvial terraces by ^{230}Th/U on pedogenic carbonate, Wind River Basin, Wyoming. Quaternary Res. 59, 139–150.
Skougstad, M.W., Horr, C.A., 1963. Occurrence and distribution of strontium in natural water. U.S. Geological Survey Water Supply Paper 1496-D, 97 p.
Spano, T., Olds, T.A., Hall, S.M., Kampf, A.R., Lowers, H., Burns, P.C., 2017. Finchite, IMA 2017–052. Mineral. Magazine 81, 1279–1286.
Steiger, R.H., Jäger, E., 1977. Subcommission on geochronology: convention on the use of decay constants in geo- and cosmochronology. Earth Planet. Sci. Lett. 36, 359–362.

Toens, P.D., 1984. Surficial Uranium Deposits. International Atomic Energy Agency IAEA-TECHDOC-322. International Atomic Energy Agency, Vienna, pp. p.
U.S. Department of Energy, 1980. An Assessment Report on Uranium in the United States of America GJO-111(80). U.S Department of Energy, Grand Junction, Colorado, pp. 148.
Van Gosen, B.S., Hall, S.M., 2017. The discovery and character of Pleistocene calcrete uranium deposits in the Southern High Plains of West Texas, United States. U.S. Geological Survey Scientific Investigations Report 2017-5134, pp. 27.
Waechter, N.B., 1974. Final Report Sulphur Springs Draw, Martin County, Texas Uranium Deposit. Internal company correspondence, Kerr-McGee Corporation, pp. 6.
Waechter, N.B., 1976. Equilibrium of Sulfur Springs Draw Mineralization. Internal company correspondence, Kerr-McGee Corporation, pp. 4.
Watanabe, Y., Nakai, S., 2006. U-Th radioactive disequilibrium analyses for JCp-1, coral reference distributed by the Geological Survey of Japan. Geochem. J. 40, 537–541.
Wetz, T.V., Reyher, S.L., 1981. Review of Kerr-McGee's West Texas Properties. Internal company correspondence, Rocky Mountain Energy, pp. 8.
Wood, W.W., 2002. Role of ground water in geomorphology, geology, and paleoclimate of the Southern High Plains, USA. Ground Water 40, 438–447.
Youlton, B., 2007. Controls on Uranium Mineralization at the Klein Trekkopje prospect, Namibia. BSc Honours thesis. University of Witwatersrand, pp. 63.
Zielinski, R.A., 1983. Tuffaceous sediments as source rock for uranium – a case study of the White River Formation, Wyoming. J. Geochem Exploration 18, 285–306.